Table 2
Summary of quantitative analysis in the cerebral cortex.

		Superior frontal cortex			Middle temporal cortex		
		Controls (mean ± SD)	XP-A (mean ± SD)	Mann–Whitney test (p value)	Controls (mean ± SD)	XP-A (mean ± SD)	Mann–Whitney test (p value)
Microtubule associated protein 2		122 ± 13	121 ± 2	ns	124 ± 8	110 ± 8	ns
Calbindin-D28K		33 ± 7	8 ± 7	<0.01	33 ± 4	9 ± 4	<0.01
	(%)	31 ± 5	12 ± 12	<0.05	27 ± 4	8 ± 3	<0.01
Parvalbumin		27 ± 4	15 ± 10	<0.05	22 ± 1	5 ± 4	<0.01
	(%)	26 ± 2	12 ± 8	<0.05	17 ± 2	5 ± 3	<0.01
Calretinin		49 ± 5	44 ± 11	ns	50 ± 7	36 ± 6	<0.05
	(%)	42 ± 5	36 ± 9	ns	41 ± 4	32 ± 5	<0.05

Abbreviations: XP-A, xeroderma pigmentosum group A; ns, not significant.

Table 3
Summary of quantitative analysis in the pedunculopontine tegmental nucleus.

		Controls (mean ± SD)	XP-A (mean ± SD)	Mann–Whitney test (p value)
Microtubule associated protein 2		244 ± 44.5	96 ± 16	<0.01
Acetylcholine esterase		68.2 ± 18	0	<0.01
	(%)	29 ± 9.6	0.2 ± 0.4	<0.01
Tyrosine hydroxylase		24.8 ± 14.6	3.4 ± 2.8	<0.01
	(%)	10.2 ± 4.8	3.3 ± 2.5	<0.05
Calbindin-D28K		26.8 ± 18.2	20 ± 12	ns
	(%)	10.7 ± 6.9	20.1 ± 12.3	ns

Abbreviations: XP-A, xeroderma pigmentosum group A; ns, not significant.

Functioning, Disability and Health scaling system significantly increased without any adverse effects in patients with Down syndrome treated with donepezil in comparison to those in placebo controls in a 24-week randomized, double-blind, placebo-controlled trial [24]. We hypothesize that donepezil may be effective for treating mental disturbances and/or REM sleep abnormalities in patients with XP-A, although donepezil has never been used in these patients.

The pathogenesis of the lesions of the cortical GABAis and AchNs in cases of XP-Ais not clear. We observed the involvement of apoptotic neuronal loss and oxidative stress with disturbed glutamate transport in the degeneration of the cerebellar cortex and the basal ganglia, respectively, in XP-A [25–27]. However, neither apoptotic neuronal loss nor oxidative stress was observed in the cerebral cortex, the NM, or the PPN. It is possible that the disturbed NER and/or null expression of XP-A protein may affect the development and/or survival of specific neuronal groups in the brain. Nevertheless, *Xpa* gene-knockout mice, an animal model of XP-A, are deficient in NER and sensitive to ultraviolet-induced skin carcinogenesis, but they are behaviorally normal and lack significant neuronal loss in the brain [28]. Further research in mice using a conditional knock-out of the *Xpa* gene in the brain may be helpful to clarify the pathogenesis of the impairment of specific neuron groups in XP-A.

References

[1] Kraemer KH, Patronas NJ, Schiffmann R, Brooks BP, Tamura D, Digiovanna JJ. Xeroderma pigmentosum, trichothiodystrophy and Cockayne syndrome: a complex genotype–phenotype relationship. Neuroscience 2007;145:1388–96.
[2] Hirai Y, Kodama Y, Moriwaki S, Noda A, Cullings HM, Macphess DG, et al. Heterozygous individuals bearing a founder mutation in the XPA DNA repair gene comprise nearly 1% of the Japanese population. Mutat Res 2006;601:171–8.
[3] Hayashi M. Role of oxidative stress in xeroderma pigmentosum. Adv Exp Med Biol 2008;637:120–7.
[4] Itoh M, Hayashi M, Shioda K, Minagawa M, Isa F, Tamagawa K, et al. Neurodegeneration in hereditary nucleotide repair disorders. Brain Dev 1999;21:326–33.
[5] Hayashi M, Araki S, Kohyama J, Shioda K, Fukatsu R, Tamagawa K. Brainstem and basal ganglia lesions in xeroderma pigmentosum group A. J Neuropathol Exp Neurol 2004;63:1048–57.
[6] Hachiya Y, Hayashi M, Kumada S, Uchiyama A, Tsuchiya K, Kurata K. Mechanisms of neurodegeneration in neuronal ceroid-lipofuscinosis. Acta Neuropathol 2006;111:168–77.
[7] Hamano K, Hayashi M, Shioda K, Fukatasu R, Mizutani S. Mechanisms of neurodegeneration in mucopolysaccharidoses II and IIIB: analysis of human brain tissue. Acta Neuropathol 2008;115:547–59.
[8] Hayashi M, Kumada S, Shioda K, Fukatsu R. Neuropathological analysis of the brainstem and cerebral cortex lesions on epileptogenesis in hereditary dentatorubral-pallidoluysian atrophy. Brain Dev 2007;29:473–81.
[9] Anzai Y, Hayashi M, Ohya T, Yokota S. The pedunculopontine nucleus in developmental disorders of the basal ganglia. Neuropathology 2008;28:258–63.

[10] Isacson O, Seo H, Lin L, Albeck D, Granholm AC. Alzheimer's disease and Down's syndrome: roles of APP, trophic factors and Ach. Trends Neurosci 2002;25:79–84.
[11] Berger-Sweeney J. The cholinergic basal forebrain system during development and its influence on cognitive processes: important questions and potential answers. Neurosci Biobehav Rev 2003;27:401–11.
[12] Kohyama J, Furushima W, Sugawara Y, Shimohira M, Hasegawa T, Hayashi M, et al. Convulsive episodes in patients with group A xeroderma pigmentosum. Acta Scand Neurol 2005;112:265–9.
[13] Olszewski J, Baxter D. Cytoarchitecture of the human brain stem. 2nd ed. New York: Karger; 1982.
[14] Prince DA, Parada I, Scalise K, Graber K, Shen F. Epilepsy following cortical injury: cellular and molecular mechanisms as targets for potential prophylaxis. Epilepsia 2009;50:30–40.
[15] Mikkonen M, Alafuzoff I, Tapiola T, Soininen H, Miettinen R. Subfield- and layer-specific changes in parvalbumin, calretinin, and calbindin-D28K immunoreactivity in the entorhinal cortex in Alzheimer's disease. Neuroscience 1999;92:515–32.
[16] Beasley CL, Zhang ZJ, Patten I, Reynolds GP. Selective deficits in prefrontal cortical GABAergic neurons in schizophrenia defined by the presence of calcium-binding proteins. Biol Psychiatry 2002;52:708–15.
[17] Lee MS, Rinne JO, Marsden CD. The pedunculopontine nucleus: its role in the genesis of movement disorders. Yonsei Med J 2000;41:167–84.
[18] Hayashi M, Miyata R, Tanuma N. Decrease in acetylcholinergic neurons in the pedunculopontine tegmental nucleus in a patient with Prader-Willi syndrome. Neuropathology 2011;31:280–5.
[19] Kohyama J, Shimohira M, Kondo S, Fukuro S, Kouji T, Sugimoto J, et al. Motor disturbances during REM sleep in group A xeroderma pigmentosum. Acta Neurol Scand 1995;92:91–5.
[20] Miyata R, Sasaki T, Hayashi M, Araki S, Shimohira M, Kohyama J. Low dose of levodopa is effective for laryngeal dystonia in xeroderma pigmentosum group A. Brain Dev 2010;32:685–7.
[21] MoraesWdos S, Povares DR, Guilleminault C, Ramos LR, Bertolucci PH, Tufik S. The effect of donepezil on sleep and REM sleep EEG in patients with Alzheimer disease: a double-blind placebo-controlled study. Sleep 2006;29:199–205.
[22] Massironi G, Galluzzi S, Frisoni GB. Drug treatment of REM sleep behavior disorders in dementia with Lewy bodies. Int Psychogeriatr 2003;15:377–83.
[23] Kishnani PS, Sommer BR, Handen BL, Seltzer B, Capone GT, Spiridigliozzi GA, et al. The efficacy, safety, and tolerability of donepezil for the treatment of young adults with Down syndrome. Am J Med Genet A 2009;149A:1641–54.
[24] Kondoh T, Kanno A, Itoh H, Nakashima M, Honda R, Kojima M, et al. Donepezil significantly improves abilities in daily lives of female Down syndrome patients with severe cognitive impairment: a 24-week randomized, double-blind, placebo-controlled trial. Int J Psychiatry Med 2011;41:71–89.
[25] Kohji T, Hayashi M, Shioda K, Minagawa M, Morimatsu Y, Tamagawa K, et al. Cerebellar neurodegeneration in human hereditary DNA repair disorders. Neurosci Lett 1998;243:133–6.
[26] Hayashi M, Itoh M, Araki S, Kumada S, Shioda K, Tamagawa K, et al. Oxidative stress and glutamate transport in hereditary nucleotide repair disorders. J Neuropathol Exp Neurol 2001;60:350–6.
[27] Hayashi M, Araki S, Kohyama J, Shioda K, Fukatsu R. Oxidative nucleotide damage and superoxide dismutase expression in the brains of xeroderma pigmentosum group A and Cockayne syndrome. Brain Dev 2005;27:34–8.
[28] Nakane H, Hirota S, Brooks PJ, Nakabeppu Y, Nakatsu Y, Nishimune Y, et al. Impaired spermatogenesis and elevated spontaneous tumorigenesis in xeroderma pigmentosum group A gene (Xpa)-deficient mice. DNA Repair 2008;7:1938–50.

NEUROPATHOLOGY

Neuropathology 2011; ••, ••–••

doi:10.1111/j.1440-1789.2011.01241.x

Original Article

Brain vascular changes in Cockayne syndrome

Masaharu Hayashi,[1] Naho Miwa-Saito,[1] Naoyuki Tanuma[1] and Masaya Kubota[2]

[1]Department of Brain Development and Neural Regeneration, Tokyo Metropolitan Institute of Medical Science and [2]Department of Neurology, National Center for Child Health and Development, Tokyo, Japan

Cockayne syndrome (CS) and xeroderma pigmentosum (XP) are caused by deficient nucleotide excision repair. CS is characterized by cachectic dwarfism, mental disability, microcephaly and progeria features. Neuropathological examination of CS patients reveals dysmyelination and basal ganglia calcification. In addition, arteriosclerosis in the brain and subdural hemorrhage have been reported in a few CS cases. Herein, we performed elastica van Gieson (EVG) staining and immunohistochemistry for collagen type IV, CD34 and aquaporin 4 to evaluate the brain vessels in autopsy cases of CS, XP group A (XP-A) and controls. Small arteries without arteriosclerosis in the subarachnoid space had increased in CS cases but not in either XP-A cases or controls. In addition, string vessels (twisted capillaries) in the cerebral white matter and increased density of CD34-immunoreactive vessels were observed in CS cases. Immunohistochemistry findings for aquaporin 4 indicated no pathological changes in either CS or XP-A cases. Hence, the increased subarachnoid artery space may have caused subdural hemorrhage. Since such vascular changes were not observed in XP-A cases, the increased density of vessels in CS cases was not caused by brain atrophy. Hence, brain vascular changes may be involved in neurological disturbances in CS.

Key words: brain vessels, CD34, Cockayne syndrome, immunohistochemistry, xeroderma pigmentosum.

INTRODUCTION

Cockayne syndrome (CS) is a rare genetic disorder caused by deficient nucleotide excision repair (NER), and it is characterized by cachectic dwarfism, mental disability, microcephaly, cerebellar ataxia, retinal pigmentation, and neural deafness.[1] Neuropathological findings of CS patients show small cerebrum, tigroid leukoencephalopathy (dysmyelination), basal ganglia calcification, cerebellar atrophy and demyelinating peripheral neuropathy.[2] Many features of CS resemble those of premature aging, and hence, CS is considered as a progeroid syndrome.[3] Nancy and Berry divided 140 published cases into three types: type I, the most prevalent classical childhood disorder; type II, an infrequent, severe congenital, or infantile variant of the disorder; type III, atypical late onset of the disorder with prolonged survival.[4]

Xeroderma pigmentosum (XP) is an inherited neurocutaneous disorder caused by defects in the NER system.[1] Complementation studies using cell hybridization assays revealed the existence of eight genes in XP (groups A–G and a variant) and two in CS (A and B). NER includes global genome repair and transcription-coupled repair (TCR), which involves several XP genes (especially *XP-A* to *XP-G*) and two CS genes (*CSA* and *CSB*). In XP, the initial presentations are skin symptoms and progressive neurological manifestations, including cognitive and motor deterioration, neuronal deafness, peripheral neuropathy and brain atrophy, mainly in XP-A, XP-B, XP-D and XP-G cases.[2] The molecular basis of CS includes recessive mutations in *CSA* (*CKN1* or *ERCC8*) and *CSB* (*CKN2* or *ERCC6*) genes, but it has not been systematically mapped to the clinical phenotypes. We investigated neurodegeneration in autopsy cases of CS and XP-A.[2]

Arteriosclerosis in the brain[5] and cerebral vascular disorders have been reported in a few cases.[6] In order to characterize the brain vascular changes in CS, we compared the immunohistochemical changes in the brain vessels between CS cases and XP-A cases as disease controls.

MATERIALS AND METHODS

Subjects

The clinical study comprised five cases of clinically and genetically confirmed CS, six cases of clinically and

Correspondence: Masaharu Hayashi, Project Leader, Department of Brain Development and Neural Regeneration, Tokyo Metropolitan Institute of Medical Science, 2-1-6, Kamikitazawa, Setagaya-ku, Tokyo 156-8506, Japan. Email: hayashi-ms@igakuken.or.jp

Received 16 May 2011; revised and accepted 31 May 2011.

Table 1 Summary of brain vascular changes in subjects

Subject	Age (years)	Sex	Cause of death	Brain weight (g)	Increase of subarachnoid small arteries	Twisted capillaries in the white matter	Density of CD34-immunoreactive vessels	
							Frontal Mean (SD)	Temporal Mean (SD)
Controls								
1	9	Male	Acute leukemia	N/A	(–)	(–)	29 (2)	21 (5)
2	13	Male	Chronic hepatitis	n/A	(–)	(–)	31 (1)	N/A
3	16	Male	Pneumonia	1505	(–)	(–)	29 (3)	25 (1)
4	20	Male	Malignant hyperthermia	N/A	(–)	(–)	26 (2)	25 (5)
5	29	Female	Guilain-Barre syndrome	N/A	(–)	(–)	38 (3)	33 (6)
6	36	Female	Thrombotic thrombocytopenic purpura	1475	(–)	(–)	37 (1)	30 (4)
7	47	Male	Acute leukemia	1400	(–)	(–)	35 (5)	38 (3)
8	55	Male	Lung cancer	N/A	(–)	(–)	38 (3)	36 (4)
9	60	Female	Breast cancer	1080	(–)	(–)	41 (7)	43 (4)
10	71	Male	Lung cancer	N/A	(–)	(–)	49 (3)	41 (4)
Cockayne syndrome								
1	7	Female	Pneumonia	295	1+	1+	44 (4)	41 (2)
2	15	Male	Renal failure	340	1+	1+	45 (4)	43 (4)
3	16	Female	Asthma	615	1+	(–)	48 (6)	N/A
4	18	Male	Renal failure	400	1+	1+	53 (5)	49 (5)
5	18	Male	Renal failure	414	1+	1+	44 (5)	45 (4)
Xeroderma pigmentosum group A								
1	19	Male	Candidiasis	580	(–)	(–)	28 (7)	26 (3)
2	19	Male	Renal failure	610	(–)	(–)	29 (11)	27 (2)
3	21	Male	Pneumonia	720	(–)	(–)	28 (3)	28 (2)
4	23	Female	Pneumonia	580	(–)	(–)	32 (2)	30 (3)
5	24	Female	Pneumonia	500	(–)	(–)	39 (4)	38 (4)
6	26	Female	Pneumonia	530	(–)	(–)	39 (3)	38 (4)

N/A, not assessed.

genetically confirmed XP-A, and 10 controls without any pathological changes in the CNS, aged 9–71 years (Table 1). The clinical and pathological findings in the CS cases 1–4 and XP-A cases 1–2 and 4–6 were reported previously.[7] The study was approved by the ethical committee of Tokyo Metropolitan Institute of Medical Science; informed consent was obtained from the patients' families before performing post mortem analyses.

Histochemistry and immunohistochemistry

The brains were fixed in buffered formalin solution; coronal sections of each formalin-fixed brain sample were cut and embedded in paraffin. Serial 6-μm-thick sections were cut from selected brain regions, including the superior frontal cortex, middle temporal cortex, basal ganglia and thalamus. HE staining and elastica van Gieson (EVG) staining were performed. After microwave antigen retrieval, each section was treated with CD34 (Nichirei, Tokyo, Japan) and rabbit polyclonal antibody to aquaporin 4 (AQP4; Santa Cruz Biotech, Santa Cruz, CA, USA). Each section was pretreated with proteinase K and mouse monoclonal antibody to collagen type IV (Col4: Sigma-Aldrich, St Louis, MO, USA). The antibody concentrations used for analysis were as follows: 1:1 (CD34), 1:100 (AQP4) and 1:500 (Col4). Antibody binding was visualized by means of the avidin–biotin immunoperoxidase complex method (Nichirei, Tokyo, Japan) according to the manufacturer's protocol.

Quantitative evaluation and data analysis

To determine the densities of the immunoreactive vessels, including arteries, veins and capillaries in the superior frontal cortex and middle temporal cortex, we determined the numbers of vessels immunoreactive for CD34 in five nonoverlapping microscopic subfields at 200-fold magnification by using a counting box (0.5 mm^2). Data were presented as mean (SD) and analyzed by nonparametric Mann–Whitney *U*-test to compare the results in different subjects. The level of significance was set at $P < 0.05$ to adjust for comparisons.

RESULTS

The results of HE and EVG staining and immunohistochemistry suggested that only CS patients had increased small arteries and arterioles in the subarachnoid space filled with fibrotic tissue and without arteriosclerosis (Table 1 and Fig. 1A). Further, small twisted and longitudinally running capillaries in cerebral white matter were observed in 4/5 CS patients but were not found in the brain

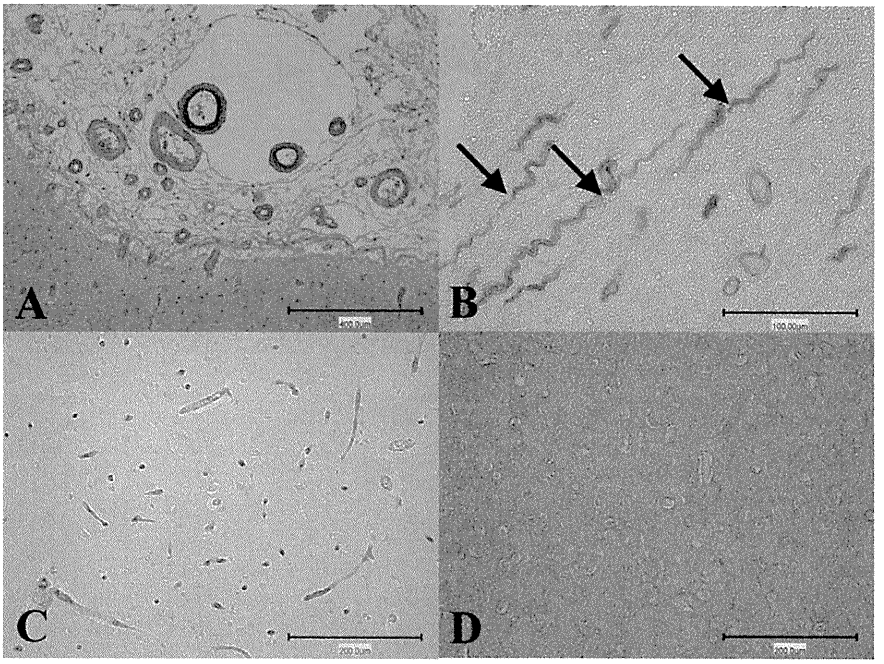

Fig. 1 Vascular changes in the brain of Cockayne syndrome (CS) patients. (A) Small arteries had increased subarachnoid space in CS case 1, elastica van Gieson staining. Bar = 400 μm. (B) Small twisted capillaries (arrows) were identified by immunostaining for collagen type IV in the cerebral white matter in CS case 4. Bar = 100 μm. (C) Vessels immunoreactive for CD34 in the middle temporal cortex in CS case 2. Bar = 200 μm. (D) Astrocyte processes were diffusely visualized by immunohistochemistry for aquaporin 4 in the cerebral white matter in CS case 4. Bar = 200 μm.

in either XP-A patients or controls (Table 1 and Fig. 1B). Twisted capillaries had more than five undulations, and were differentiated from functioning capillaries. In controls, the density of CD34-immunoreactive vessels in the frontal and temporal cortex of aged subjects was one-and-half times higher than that in teenagers, suggesting that the increase was age-dependent (Table 1). The density of CD34-immunoreactive vessels in CS cases aged less than 20 years was over 40 (Fig. 1C), which was equal to that in aged controls. The mean (SD) was 32 (4) in controls aged from 9 to 36 years, 47 (3) in CS cases, and 33 (5) in XP-A cases in the superior frontal cortex, respectively. The mean (SD) was 27 (4) in controls aged from 9 to 36 years, 45 (3) in CS cases, and 31 (5) in XP-A cases in the middle temporal cortex, respectively. The density of CD34-immunoreactive vessels in CS cases was significantly higher than those in controls and XP-A patients ($P < 0.05$). Furthermore, in CS patients, the number of capillaries increased around the calcified foci in the basal ganglia (data not shown). The vessel wall calcification was not found in the cerebral cortex, white matter or subarachnoid space. AQP4 immunostaining visualized the astrocyte processes around the vessels in all subjects (Fig. 1D) and there were no pathological changes in either CS or XP-A patients.

DISCUSSION

Cockayne syndrome and XP-A patients had severe brain atrophy (Table 1) and fibrosis in the enlarged subarachnoid space. However, the number of arteries and arterioles increased only in CS patients, suggesting excessive branching in the cortical arteries in CS. Similarly, in the subarachnoid space, increased density of CD34-immunoreactive vessels in the frontal and temporal cortex was observed in CS but not in XP-A patients. The reduction of brain area due to brain atrophy possibly leads to the apparent increase in the density of vessels. Nevertheless, since there was no increase in density in XP-A patients, the increased density of vessels in CS patients was not caused by the brain atrophy. Subdural hemorrhage is usually caused by tearing of the bridging cortical veins after head trauma, but traumatic aneurysms in the cortical arteries are a rare cause of such hemorrhages.[8] The increased number of subarachnoid and/or intracortical arteries may be a risk factor for subdural hemorrhage, which has been reported in CS patients.[6] A recent study showed that *CSB* mutant cells did not exhibit a normal reaction to hypoxia; these cells did not activate hypoxia-inducible factor-1 on the promoter gene due to which downstream events such as transcription factor IIB (TFIIB) recruitment did not occur.[9] Insufficient hypoxic response may disturb the induction of growth factors such as VEGF, suggesting the possible involvement of angiogenesis in CS. The analysis of brain vessels in fetal autopsy cases of CS might reveal the disturbances of angiogenesis during brain development.

Rapin *et al.* reported twisted microvessels consistent with so-called string vessels in the brains of adult CS patients.[5] We observed a similar morphological change in CS patients in our analysis. The absence of twisted microvessels in XP-A patients is noteworthy, and deficient NER is unlikely to have direct relationships with the

vascular changes in CS patients. Brooks *et al.* stressed that in addition to brain vascular lesions, there is an overlap in neurological symptoms, such as dysmyelination and brain calcification between CS and Aicardi–Goutières syndrome. They proposed that the vascular changes probably occur due to alterations in gene expression and may play a role in the generation of neurological abnormalities in both the diseases.[10]

CS is considered to be a progeroid condition since many symptoms of CS resemble premature aging. It is intriguing that arteriosclerosis was absent in the brain vessels in our CS patients, although this change has been pointed out in CS cases reported in the literature. In good accordance of our findings, the absence of atherosclerotic changes in the systemic arteries was reported in a 40-year-old patient with CS of probable type III.[11] Furthermore, neither senile plaques nor vascular beta-amyloid depositions were identified in the temporal lobe in three patients with CS of probably type I or II, two aged 2 and one aged 6 years, respectively.[12] In Werner syndrome (WS) associated with supposed accelerated aging, patients rarely show age-associated neuropathology and lack amyloid deposition, indicating the absence of extension of WS-associated aging in the CNS.[13] Although the increased occurrence of arteriosclerosis in the heart, aorta and kidney is a definite characteristic of CS and WS, further analysis of many autopsy cases is required to verify the facilitation of brain arteriosclerosis in both the disorders.

Mouse models for CS-A and CS-B show a TCR defect and increased photosensitivity in the skin. However, growth failure and neurological abnormalities are not predominant.[14,15] $Csb^{m/m}/Xpa^{-/-}$ double mutant animals show post natal growth retardation, ataxia, abnormal locomotor activity, progressive weight loss and early death.[16] However, in these model animals, brain vascular changes have not been examined in detail. Complete inactivation of NER by deletion of *XP-A* gene in animals does not cause CS-like neurodevelopmental and progeroid features, and it has been proposed that some of the CS features may be the outcome of defects in the transcription function of transcription/repair factor TFIIH and/or defective repair of oxidative DNA lesions.[17] We have investigated the involvement of oxidative stress in the brains of XP-A and CS autopsy cases.[2] Lipid peroxidation and protein glycation markers were found in the perivascular calcification areas in the globus pallidus and cerebellum more predominantly in CS than in XP-A patients. We found a similar deposition of oxidative stress markers in the calcification areas in the brain vessel walls in cases of pseudohypoparathyroidism and Fahr disease.[18] Since increased oxidative stress is known to cause vascular calcifications in bone and kidney diseases,[19,20] it is possible that oxidative stress may be involved in the generation of brain vascular changes in CS.

Our findings suggest that vascular changes in the brain may be involved in neurological disturbances in CS. A detailed investigation of the brain vessels may help us clarify the pathogenesis of neurological abnormalities.

REFERENCES

1. Kraemer KH, Patronas NJ, Schiffmann R, Brooks BP, Tamura D, Digiovanna JJ. Xeroderma pigmentosum, trichothiodystrophy and Cockayne syndrome: a complex genotype–phenotype relationship. *Neuroscience* 2007; **145**: 1388–1396.
2. Hayashi M. Role of oxidative stress in xeroderma pigmentosum. *Adv Exp Med Biol* 2008; **637**: 120–127.
3. Martin GM. Genetic modulation of senescent phenotypes in Homo sapiens. *Cell* 2005; **120**: 523–532.
4. Nance MA, Berry SA. Cockayne syndrome: review of 140 cases. *Am J Med Genet* 1992; **42**: 68–84.
5. Rapin I, Weidenheim K, Lindenbaum Y *et al.* Cockayne syndrome in adults: review with clinical and pathologic study of a new case. *J Child Neurol* 2006; **21**: 991–1006.
6. Shimoizumi H, Matsui M, Ito S, Miyao M, Kobayashi S. Cockayne syndrome complicated by acute subdural hemorrhage. *Brain Dev* 1995; **17**: 376.
7. Itoh M, Hayashi M, Shioda K *et al.* Neurodegeneration in hereditary nucleotide repair disorders. *Brain Dev* 1999; **21**: 326–333.
8. Cho WS, Batchuluun B, Lee SJ, Kang HS, Kim JE. Recurrent subdural hematoma from a pseudoaneurysm at the cortical branch of the middle artery after mild head injury: case report. *Neurol Med Chir (Tokyo)* 2011; **51**: 217–221.
9. Filippi S, Latini P, Frontini M, Palitti F, Egly JM, Proietti-De-Santis L. CSB protein is (a direct target of HIF-1 and) a critical mediator of the hypoxic response. *EMBO J* 2008; **27**: 2545–2556.
10. Brooks PJ, Cheng TF, Cooper L. Do all of the neurologic diseases in patients with DNA repair gene mutations result from the accumulation of DNA damage? *DNA Repair* 2008; **7**: 834–848.
11. Inoue T, Sano N, Ito Y *et al.* An adult case of Cockayne syndrome without sclerotic angiopathy. *Intern Med* 1997; **36**: 565–570.
12. Woody RC, Harding BN, Brumback RA, Leech RW. Absence of β-amyloid immunoreactivity in mesial temporal lobe in Cockyane's syndrome. *J Child Neurol* 1991; **6**: 32–34.
13. Mori H, Tomiyama T, Maeda N, Ozawa K, Wakasa K. Lack of amyloid plaque formation in the central nervous system of a patient with Werner syndrome. *Neuropathology* 2003; **23**: 51–56.

14. van der Horst GT, Meira L, Gorgels TG *et al.* UVB radiation-induced cancer predisposition in Cockayne syndrome group A (Csa) mutant mice. *DNA Repair* 2002; **1**: 143–157.
15. van der Horst GT, van Steeg H, Berg RJ *et al.* Defective transcription-coupled repair in Cockayne syndrome B mice is associated with skin cancer predisposition. *Cell* 1997; **89**: 425–435.
16. Murai M, Enokido Y, Inamura N *et al.* Early postnatal ataxia and abnormal cerebellar development in mice lacking seroderma pigmentosum group A and Cockayne syndrome group B DNA repair genes. *Proc Natl Acad Sci U S A* 2001; **98**: 13379–13384.
17. Andressoo JO, Weeda G, de Wit J *et al.* An Xpb mouse model for combined xeroderma pigmentosum and Cockayne syndrome reveals progeroid features upon further attenuation of DNA repair. *Mol Cell Biol* 2009; **29**: 1276–1290.
18. *Neurodegenerative Diseases*, edited by Shamim I. Ahmad, from Landes Bioscience and Springer Science (ISBN: 978-1-4614-0652-5). http://www.landesbioscience.com/books/special/id/4242/
19. Mody N, Parhami F, Sarafian TA, Demer LL. Oxidative stress modulates osteoblastic differentiation of vascular and bone cells. *Free Radic Biol Med* 2001; **31**: 509–519.
20. Massy ZA, Maziere C, Kamel S *et al.* Impact of inflammation and oxidative stress on vascular calcifications in chronic kidney disease. *Pediatr Nephrol* 2005; **20**: 380–382.

Augmented cell death with Bloom syndrome helicase deficiency

HIDEO KANEKO[1,2], TOSHIYUKI FUKAO[1], KIMIKO KASAHARA[1], TAKETO YAMADA[3] and NAOMI KONDO[1]

[1]Department of Pediatrics, Graduate School of Medicine, Gifu University, Gifu 501-1194; [2]Department of Clinical Research, Nagara Medical Center, Gifu 502-8558; [3]Department of Pathology, School of Medicine, Keio University, Tokyo 160-8582, Japan

Received December 20, 2010; Accepted March 28, 2011

DOI: 10.3892/mmr.2011.484

Abstract. Bloom syndrome (BS) is a rare autosomal genetic disorder characterized by lupus-like erythematous telangiectasias of the face, sun sensitivity, infertility, stunted growth, upper respiratory infection, and gastrointestinal infections commonly associated with decreased immunoglobulin levels. The syndrome is associated with immunodeficiency of a generalized type, ranging from mild and essentially asymptomatic to severe. Chromosomal abnormalities are hallmarks of the disorder, and high frequencies of sister chromatid exchanges and quadriradial configurations in lymphocytes and fibroblasts are diagnostic features. BS is caused by mutations in BLM, a member of the RecQ helicase family. We determined whether BLM deficiency has any effects on cell growth and death in BLM-deficient cells and mice. BLM-deficient EB-virus-transformed cell lines from BS patients and embryonic fibroblasts from $BLM^{-/-}$ mice showed slower growth than wild-type cells. BLM-deficient cells showed abnormal p53 protein expression after irradiation. In $BLM^{-/-}$ mice, small body size, reduced number of fetal liver cells and increased cell death were observed. BLM deficiency causes the up-regulation of p53, double-strand break and apoptosis, which are likely observed in irradiated control cells. Slow cell growth and increased cell death may be one of the causes of the small body size associated with BS patients.

Introduction

Bloom syndrome (BS) is a rare genetic disorder caused by mutations in BLM, a member of the RecQ helicase family (1). There are five human RecQ-like proteins (RECQL1, BLM, WRN, RECQL4 and RECQ5), each having 3' to 5' DNA helicase activity, but little sequence similarity outside the helicase motifs (2,3). Three of these helicases (BLM, WRN and Rothmund-Thomson) show genomic instability and cancer susceptibility; however, each also has distinctive features (4,5). The unique features of BS are severe pre- and post-natal growth retardation and a wide spectrum of cancer types that develop at a young age. Other BS phenotypes include facial sun sensitivity, immunodeficiency and male sterility/female subfertility (6,7). Compared with Werner syndrome, small body size is one of the characteristic features associated with BS patients.

Here, we determined whether BLM deficiency has any effects on the cell growth and death of BLM-deficient cells and mice.

Materials and methods

BS patient. AsOk, who was identified in the BS registry as number 97, weighed 2,250 g at birth. Café-au-lait spots and mandibular hypoplasia were prominent. A 3-bp deletion was detected in the BLM sequence of AsOk DNA (8). This deletion caused the generation of a stop codon at amino acid 186.

Cell culture. EB-virus-transformed cell lines from BS patients and control subjects were developed as previously reported (9). In brief, PBMCs were isolated from the heparinized blood of patients by gradient centrifugation in Ficoll-Paque (Pharmacia AB, Uppsala, Sweden), and suspended at a density of 10^6 ml in culture medium consisting of RPMI 1640 supplemented with 10% heat-inactivated fetal calf serum, l-glutamine (2 mmol/l), penicillin (100 U/ml) and streptomycin (100 μg/ml). The PBMCs (10^6 ml) were then cultured in the presence of 10 μg/ml phytohemagglutinin (PHA) for 3 days.

Detection of p53 protein. PBMCs cultured with PHA for 3 days were irradiated (6 Gy). After 1 h, the cells were collected by centrifugation and protein was extracted. Using anti-human p53 antibody (Santacruz, USA), immunoblotting was performed.

BLM-deficient embryonic fibroblasts. Heterozygous BLM-deficient ($BLM^{+/-}$) mice were kindly provided by P. Leder. $BLM^{-/-}$ mice were obtained by mating $BLM^{+/-}$ mice (10). Embryonic fibroblasts from $BLM^{-/-}$ mice were obtained from 12.5-day embryos. None of the $BLM^{-/-}$ embryos survived more than 13 days.

Cell proliferation assay. Cell proliferation and cell viability were determined by the trypan blue or MTT assays. The MTT assay was performed following the manufacturer's protocol.

Correspondence to: Professor Hideo Kaneko, Department of Pediatrics, Graduate School of Medicine, Gifu University, 1-1 Yanagido, Gifu 501-1194, Japan
E-mail: hideo@gifu-u.ac.jp

Key words: Bloom syndrome, small body size, BLM deficiency, cell death

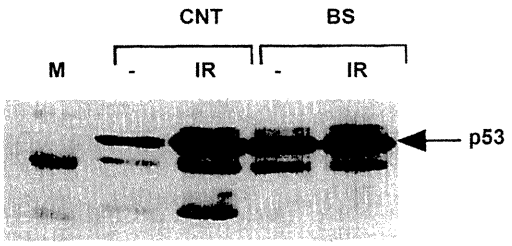

Figure 1. p53 protein expression in PBMCs from a control subject and a BS patient. PBMCs cultured with PHA for 3 days were irradiated (6 Gy). After 1 h, the cells were collected and p53 protein expression was detected.

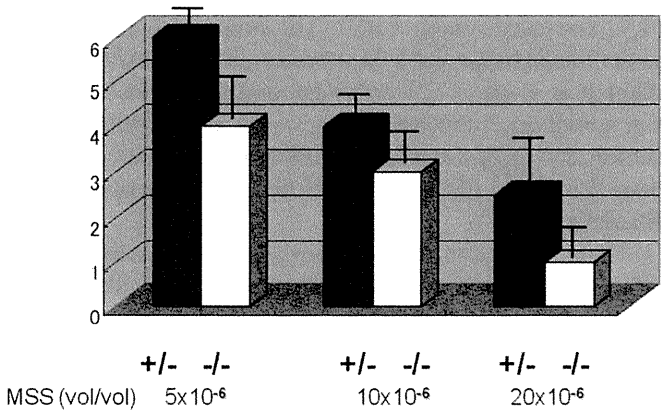

Figure 2. Fig. 2 Cell proliferation and cell viability were determined using trypan blue. Embryonic fibroblasts were established from $BLM^{-/-}$ and $BLM^{+/-}$ mice at 12.5 days post-coitus. Embryonic fibroblasts from $BLM^{-/-}$ mice showed a slow growth rate and a high sensitivity to MMS compared to those from $BLM^{+/-}$ mice.

Embryonic fibroblasts were cultured with methyl methanesulfonate (MMS) (Sigma, Japan) for 24 h (11), then the viable cell number was determined on trypan blue.

Detection of single-strand DNA. Paraffin and cryostat sections were prepared from the brain of $BLM^{+/-}$ or $BLM^{-/-}$ mice at 12.5 days post-coitus. Polyclonal rabbit anti-ssDNA antibody (IgG, 100 μg/ml, Dako Japan, Kyoto, Japan) at a dilution of 1:300 was used to detect the formation of single-stranded DNA (ssDNA) for 1 h at room temperature. Immunoreactivity was detected with peroxidase-labeled goat anti-rabbit immunoglobulins.

Results

Abnormal regulation of p53 protein expression. After the irradiation of PHA-stimulated PBMCs, p53 protein expression was induced in control cells (Fig. 1). In the PBMCs of the BS patient, high p53 protein expression was detected even without irradiation. Irradiation slightly induced p53 protein in BS cells. In the BS EB cell line, p53 phosphorylation by ATM was up-regulated compared with that in the control EB cell line (data not shown). These results suggested that BLM-deficient cells have abnormal regulation of p53 protein expression and an elevated frequency of apoptosis. Next, apoptosis was investigated *in vivo* and *in vitro* using BLM-deficient cells.

Slow growth in BLM-deficient cells. The growth rate of EB cells from BS patients was slower than that of control cells. After irradiation, the growth rate of BS cells was slower than that of control cells. MMS action caused double-stranded DNA breaks. The sensitivity of $BLM^{-/-}$ cells to MMS was higher than that of wild type cells. Embryonic fibroblasts originating from $BLM^{-/-}$ mice also showed a slowed growth rate (Fig. 2).

Augmented cell death in embryonic brain of $BLM^{-/-}$ mice. Anti-single-stranded DNA was detected in the brain of $BLM^{-/-}$ mice, with the number being higher than that detected in the brain of $BLM^{+/-}$ mice (Fig. 3). This result suggested the occurence of augmented cell death in $BLM^{-/-}$ mice.

Discussion

In this study, we showed the abnormal regulation of p53 protein expression and augmented cell death in BLM-deficient cells both *in vitro* and *in vivo*. Stalled replication forks can result in double-strand breaks, thereby triggering the activation of ATM (12). Consistent with a previously reported study, the deficiency of BLM was radiomimetic (13).

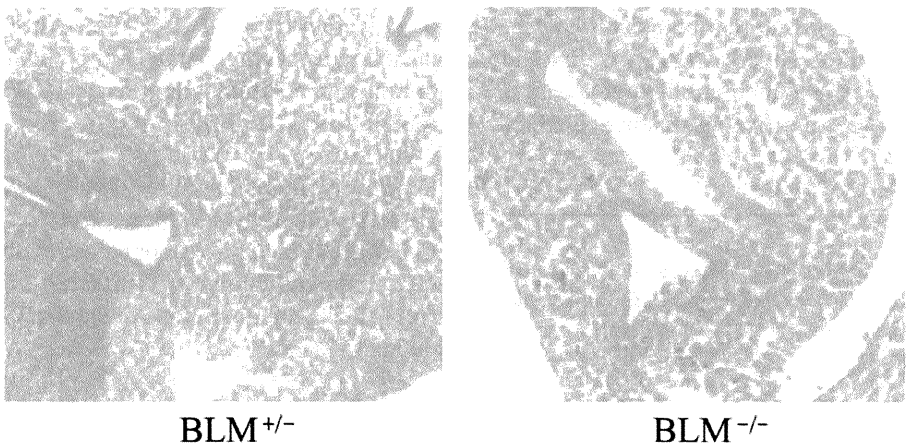

Figure 3. Detection of single-stranded DNA. Immunohistochemical staining of $BLM^{+/-}$ and $BLM^{-/-}$ embryos at 12.5 days post-coitus was performed.

Originally, MMS was considered to directly cause double-stranded DNA breaks, since homologous-recombination-deficient cells are particularly vulnerable to the effects of MMS. However, it is now considered that MMS stalls replication forks, and cells that are homologous-recombination-deficient have difficulty repairing the damaged replication forks.

Studies in yeast and human cells suggest a pivotal role of RECQ-like helicases in maintaining genomic integrity during the S phase (14). BS patients show small body size from birth. This small body size persists throughout their lifetime. At 12.5 days post-coitus, BLM-deficient mice have a smaller body size than wild-type mice (10).

BLM deficiency renders cells highly susceptible to apoptosis, which is a possible explanation for the pre- and post-natal growth retardation observed in BS patients. In the absence of BLM, many cells fail to repair damage rapidly enough, whereupon p53 signals those cells to die. Individuals with BS may continually lose cells, owing to excessive apoptosis, particularly during pre- and post-natal development, when cell proliferation is excessive (15). Excessive apoptosis would leave many tissues with chronic cellular insufficiency, and hence a small size, thereby explaining the pre- and post-natal growth retardation.

p53 is crucial for the apoptosis of BS cells. This apoptosis is not accompanied by an increase in BAX or p21 protein expression. Thus, p53 may induce apoptosis independent of its transactivation activity, consistent with the finding that p53 is transcriptionally inactive during the S phase. p53 may mediate the death of damaged BS cells by directly inducing mitochondria-mediated apoptosis, or by means of its transactivation activity.

In conclusion, BLM deficiency causes the dysregulation of p53 and augmented apoptosis, similar to that observed in irradiated wild-type cells. This slow cell growth and increased cell death may cause the small body size associated with BS patients.

Acknowledgements

This study was supported in part by Health and Labor Science Research Grants for Research on Intractable Diseases from The Ministry of Health, Labor and Welfare of Japan.

References

1. Ellis NA, Groden J, Ye TZ, *et al*: The Bloom's syndrome gene product is homologous to RecQ helicases. Cell 83: 655-666, 1995.
2. Ellis NA, Sander M, Harris CC and Bohr VA: Bloom's syndrome workshop focuses on the functional specificities of RecQ helicases. Mech Ageing Dev 129: 681-91, 2008.
3. Rossi ML, Ghosh AK and Bohr VA: Roles of Werner syndrome protein in protection of genome integrity. DNA Repair: Jan 13, 2010 (E-pub ahead of print).
4. German J: Bloom syndrome: a Mendelian prototype of somatic mutational disease. Medicine 72: 393-406, 1993.
5. Kaneko H and Kondo N: Clinical features of Bloom syndrome and function of the causative gene, BLM helicase. Expert Rev Mol Diagn 4: 393-401, 2004.
6. German J: Bloom's syndrome. Dematol Cli 13: 7-18, 1995.
7. German J and Ellis NA: Bloom syndrome. In: The Genetic Basis of Human Cancer. 1st edition. Vogelstein B and Kinzler (eds) McGraw Hill, New York, NY, pp301-315, 1998.
8. Kaneko H, Isogai K, Fukao T, *et al*: Relatively common mutations of the Bloom syndrome gene in the Japanese population. Int J Mol Med 14: 439-42, 2004.
9. Kaneko H, Matsui E, Fukao T, Kasahara K. Morimoto W and Kondo N: Expression of BLM gene in human hematopoietic cells. Clin Exp Immunol 118: 285-289, 1999.
10. Chester N, Kuo F, Kozak C, O'Hara CD and Leder P: Stage-specific apoptosis, developmental delay, and embryonic lethality in mice homozygous for a targeted disruption in the murine Bloom's syndrome gene. Genes Dev 12: 3382-3393, 1998.
11. Lundin C, North M, Erixon K, Walters K, Jenssen D, Goldman ASH and Helleday T: Methyl methanesulfonate (MMS) produces heat-labile DNA damage but no detectable in vivo DNA double-strand breaks. Nucleic Acids Res 33: 3799-3811, 2005.
12. Beamish H, Kedar P, Kaneko H, *et al*: Functional link between BLM defective in Bloom's syndrome and the ataxia-telangiectasia mutated protein, ATM. J Biol Chem 277: 30515-30523, 2002.
13. Horowitz DP, Topaloglu O, Zhang Y and Bunz F: Deficiency of Bloom syndrome helicase activity is radiomimetic. Cancer Biol Ther 7: 1783-1786, 2008.
14. Oh SD, Lao JP, Hwang PY, Taylor AF, Smith GR and Hunter N: BLM ortholog, Sgs1, prevents aberrant crossing-over by suppressing formation of multichromatid joint molecules. Cell 130: 259-272, 2007.
15. Dvalos AR and Campis J: Bloom syndrome cells undergo p53-dependent apoptosis and delayed assembly of BRCA1 and NSB1 repair complexes at stalled replication forks. J Cell Biol 29: 1197-1209, 2003.

Onset of Quiescence Following p53 Mediated Down-Regulation of H2AX in Normal Cells

Yuko Atsumi[1☯], Hiroaki Fujimori[1,3☯], Hirokazu Fukuda[2☯], Aki Inase[2], Keitaro Shinohe[3], Yoshiko Yoshioka[3], Mima Shikanai[3], Yosuke Ichijima[3], Junya Unno[4], Shuki Mizutani[4], Naoto Tsuchiya[2], Yoshitaka Hippo[2], Hitoshi Nakagama[2], Mitsuko Masutani[1], Hirobumi Teraoka[3], Ken-ichi Yoshioka[1,3]*

1 Division of Genome Stability Research, National Cancer Center Research Institute, Tokyo, Japan, **2** Division of Cancer Development System, National Cancer Center Research Institute, Tokyo, Japan, **3** Department of Pathological Biochemistry, Medical Research Institute, Tokyo Medical and Dental University, Tokyo, Japan, **4** Department of Pediatrics and Developmental Biology, Graduate School of Medical and Dental Sciences, Tokyo Medical and Dental University, Tokyo, Japan

Abstract

Normal cells, both *in vivo* and *in vitro*, become quiescent after serial cell proliferation. During this process, cells can develop immortality with genomic instability, although the mechanisms by which this is regulated are unclear. Here, we show that a growth-arrested cellular status is produced by the down-regulation of histone H2AX in normal cells. Normal mouse embryonic fibroblast cells preserve an H2AX diminished quiescent status through p53 regulation and stable-diploidy maintenance. However, such quiescence is abrogated under continuous growth stimulation, inducing DNA replication stress. Because DNA replication stress-associated lesions are cryptogenic and capable of mediating chromosome-bridge formation and cytokinesis failure, this results in tetraploidization. Arf/p53 module-mutation is induced during tetraploidization with the resulting H2AX recovery and immortality acquisition. Thus, although cellular homeostasis is preserved under quiescence with stable diploidy, tetraploidization induced under growth stimulation disrupts the homeostasis and triggers immortality acquisition.

Citation: Atsumi Y, Fujimori H, Fukuda H, Inase A, Shinohe K, et al. (2011) Onset of Quiescence Following p53 Mediated Down-Regulation of H2AX in Normal Cells. PLoS ONE 6(8): e23432. doi:10.1371/journal.pone.0023432

Editor: Michael Polymenis, Texas A&M University, United States of America

Received April 11, 2011; **Accepted** July 17, 2011; **Published** August 12, 2011

Funding: This study was supported by MEXT KAKENHI (20770136 and 20659047). The funders had no role in study design, data collection and analysis, decision to publish, or preparation of the manuscript.

Competing Interests: The authors have declared that no competing interests exist.

* E-mail: kyoshiok@ncc.go.jp

☯ These authors contributed equally to this work.

Introduction

Cancer is a disease associated with genomic instability and the accumulation of mutations [1]. Unlike specific chromosomal translocation-associated tumors, most cancers associated with aging develop either chromosomal instability (CIN) or microsatellite instability (MIN) [2]. While MIN is associated with mismatch repair deficiency, CIN develops even in a normal background [3]. However, the mechanisms by which CIN and MIN develop remain elusive.

A recent genomic analysis of various cancers revealed that massive genomic rearrangements, including loss of heterozygosity (LOH) and chromosomal translocation, amplification and deletion, do not gradually accumulate over time, as conventionally thought, but appear to be acquired in a single catastrophic event [4]. One of such events could be associated with tetraploidization because tetraploidy is a common early event in cancer cells with CIN [5]. Tetraploidy is observed in cells during the initial stages of cancer [6,7] as well as in precancerous stages such as dysplasia [8,9], but not in malignant cancer cells, which usually exhibit aneuploidy in association with deploidization [5]. Furthermore, analogous to changes observed in cancer genomes, the immortalization of mouse embryonic fibroblasts (MEFs) occurs with tetraploidy and mutation of the Arf/p53 module, which eventually evolves into aneuploidy during serial cultivation [10].

In the initial stages of carcinogenesis, cells are subjected to oncogenic stress, resulting in the accumulation of DNA replication stress-associated lesions and the onset of barrier responses such as senescence and apoptosis [11,12]. This effect can be reproduced *in vitro* by the activation of oncogenes [11] and accelerated growth stimulation [12] due to the induction of accelerated S-phase entry and the resulting DNA replication stress. Importantly, genomic instability is generated under these conditions [11,12] because DNA replication stress-associated lesions persist into M phase and mediate chromosomal bridge formation and cytokinesis failure, resulting in tetraploidization [10]. In fact, tetraploidization of MEFs is induced via chromosomal bridge formation prior to the onset of immortality with mutation of Arf/p53 [10], although it is still unclear how tetraploidization induces immortality. Since such tetraploidization is specifically observed during senescence, tetraploidization might be a defect that occurs during cell proliferation or growth arrest. In fact, similar to cells in the initial stages of carcinogenesis, senescent cells often accumulate irreparable DNA lesions [13,14] and frequently exhibit genomic instability [15].

The development of cancer, as well as the onset of immortality in cells *in vitro*, is tightly associated with mutations in the Arf/p53 module [16–18]. Although this is ascribed to the role of p53 in

cancer prevention, the regulation and roles of p53 are complex [18]. While constitutively active p53 mediates premature aging in mice [19–21], additional single gene copies of *Arf* and *p53* under functional regulation mediate longevity and cancer prevention [22]. Similarly, while the accumulation of p53 induces cellular senescence and apoptosis [16,17], additional single gene copies of *Arf* and *p53* in MEFs has a protective effect from immortalization [22], suggesting that they help to maintain homeostasis under undamaged conditions. This raises the questions of the identity of the regulatory target of p53 in preserving cellular homeostasis under normal conditions and how cellular homeostasis preservation and abrogation are associated with genomic status and p53 regulation.

This study focused on the mechanism by which normal cells under serial proliferation regulate homeostasis preservation and abrogation and sought to identify the regulatory target of p53. Our results illustrated two distinct conditions that could result in growth-arrested cells: (i) cells that maintain continuous quiescence by down-regulating H2AX (a variant of core histone H2A) under p53 regulation and stable-diploidy maintenance; and (ii) cells that develop tetraploidy and immortality under continuous growth stimulation, characterized by the accumulation of γH2AX foci. Thus, oncogenic stress under growth stimulation triggers catastrophic tetraploidization that leads to immortalization in association with the accompanying mutation of the Arf/p53 module and recovery of H2AX expression and growth activity.

Results

Immortality is prevented in quiescent cells that maintain genomic stability

MEFs cultured under the standard 3T3 protocol (Std-3T3) senesce in association with oxygen sensitivity [23], which is followed by the development of immortality with tetraploidy [10] and mutation of the Arf/p53 module [22], similar to the process of carcinogenesis. In addition, similar to cells in the initial stages of carcinogenesis, spontaneous DNA lesions accumulate in senescent MEFs under Std-3T3 conditions prior to the development of immortality [10], which suggests that growth stimulation induced under Std-3T3 conditions might overwhelm senescent MEFs. Therefore, MEFs under Std-3T3 conditions were compared with MEFs exposed to temporary serum deprivation (tSD-3T3), which induces occasional growth arrest (Fig. 1A). Under Std-3T3 conditions, MEFs were immortalized with tetraploidy that progresses to aneuploidy (Fig. 1A–C). On the other hand, MEFs cultured under tSD-3T3 conditions never developed immortality and preserved quiescence with stable diploidy (Fig. 1A, C). This indicates that temporal growth arrest prevents immortalization and supports genomic stability. Conversely, continuous culture with 10% FBS produces oncogenic stress in senescent MEFs, triggering tetraploidization. Thus, even though both are growth arrested (at least in total cell numbers) with senescent morphology at the same culture passage (P9) (Fig. S1), MEFs under tSD-3T3 conditions are continuously quiescent with genomic stability, while MEFs under Std-3T3 conditions develop tetraploidy (Fig. 1A, C), posing a question in DNA lesion status that induces chromosomal bridge formation and tetraploidization [10].

γH2AX foci accumulate in cells developing genomic instability but not in cells preserving diploidy

To determine the DNA lesion status induced by accelerated growth stimulation, γH2AX foci were compared in growth-arrested MEFs (P9) under both conditions (Fig. 1D). As expected, MEFs that developed tetraploidy under Std-3T3 conditions accumulated γH2AX foci, with some carrying over into the G2/M phases (Fig. 1E). This resulted in chromosome bridge formation (Fig. 1F) with the resulting tetraploidization that is initially observed with binucleated tetraploidy (Fig. 1F). On the other hand, quiescent MEFs that preserved genomic stability under tSD-3T3 conditions did not develop γH2AX foci (Fig. 1D), indicating that genomic stability is preserved under no γH2AX signal. However, it was still unclear why quiescent MEFs under tSD-3T3 conditions do not accumulate γH2AX foci because senescent cells are known to generally accumulate irreparable DNA lesions [13,14].

To address why γH2AX foci do not form under tSD-3T3 conditions, the expression level of H2AX at P9 was determined. As shown in Figure 1G, a remarkable reduction in H2AX expression was observed in quiescent MEFs at P9 while MEFs that developed tetraploidy under Std-3T3 conditions showed significantly higher H2AX expression than quiescent MEFs. This illustrates an association between H2AX levels and the cellular and genomic status, in that cells with largely diminished H2AX expression preserve stable diploidy and a quiescent status, while cells with residual H2AX expression and with γH2AX foci develop genomic instability and immortality (Fig. 1H). Importantly, H2AX-KO cells exhibited impaired DNA repair, growth retardation, and elevated genomic instability [24–28], phenotypes reminiscent of senescent cells. Therefore, it will be critical to determine how H2AX-status is regulated to produce quiescence and induce genomic instability.

H2AX is generally diminished in quiescent cells

To address whether H2AX diminution is a general occurrence, H2AX expression was compared in normal human fibroblasts (NHFs) and MEFs. Decreased H2AX was observed in both cell types at growth-arrested stage after serial proliferation (Fig. 2A, B), suggesting that this process is conserved between humans and mice. In addition, H2AX diminution was also observed in many organs of adult mice, including the liver, spleen, and pancreas (Fig. 2C, D; Fig. S2). Thus, H2AX is generally reduced in quiescent cell chromosomes both *in vitro* and *in vivo*.

H2AX is also diminished during premature senescence induced by DNA damage. Using early passage MEFs (P2), H2AX diminution was observed when senescence was induced by treatment with hydroxyurea (HU) to induce DNA replication stress (Fig. 2E) and with the radiomimetic DNA-damaging agent, neocarzinostatin (Fig. S3). This most likely occurs because DNA repair is coupled with H2AX release and chromatin remodeling [29–31]. Together with results showing a decrease in H2AX transcript levels in senescent MEFs (Fig. S4), these results indicate that decreased amounts of H2AX protein in senescing cells is ascribed to a decrease in H2AX transcript levels and DNA damage.

To directly address the impact of H2AX reduction, H2AX was knocked down in early passage NHFs, which induced cellular quiescence with senescent cell characteristics; cells adopted a flattened and enlarged morphology and showed an increase in senescence-associated β-galactosidase activity (Fig. 2F). Since the knockdown of H2AX in 293T cells induced growth arrest without inducing a senescent morphology (data not shown), it is likely that the effect of H2AX diminution is primarily due to quiescence induction and potentially a normal consequence of senescence in normal cells.

Immortalized cells develop following tetraploidization when H2AX status and growth activity are restored

The above results illustrate that cellular quiescence is produced when cells maintain stable diploidy and diminished H2AX

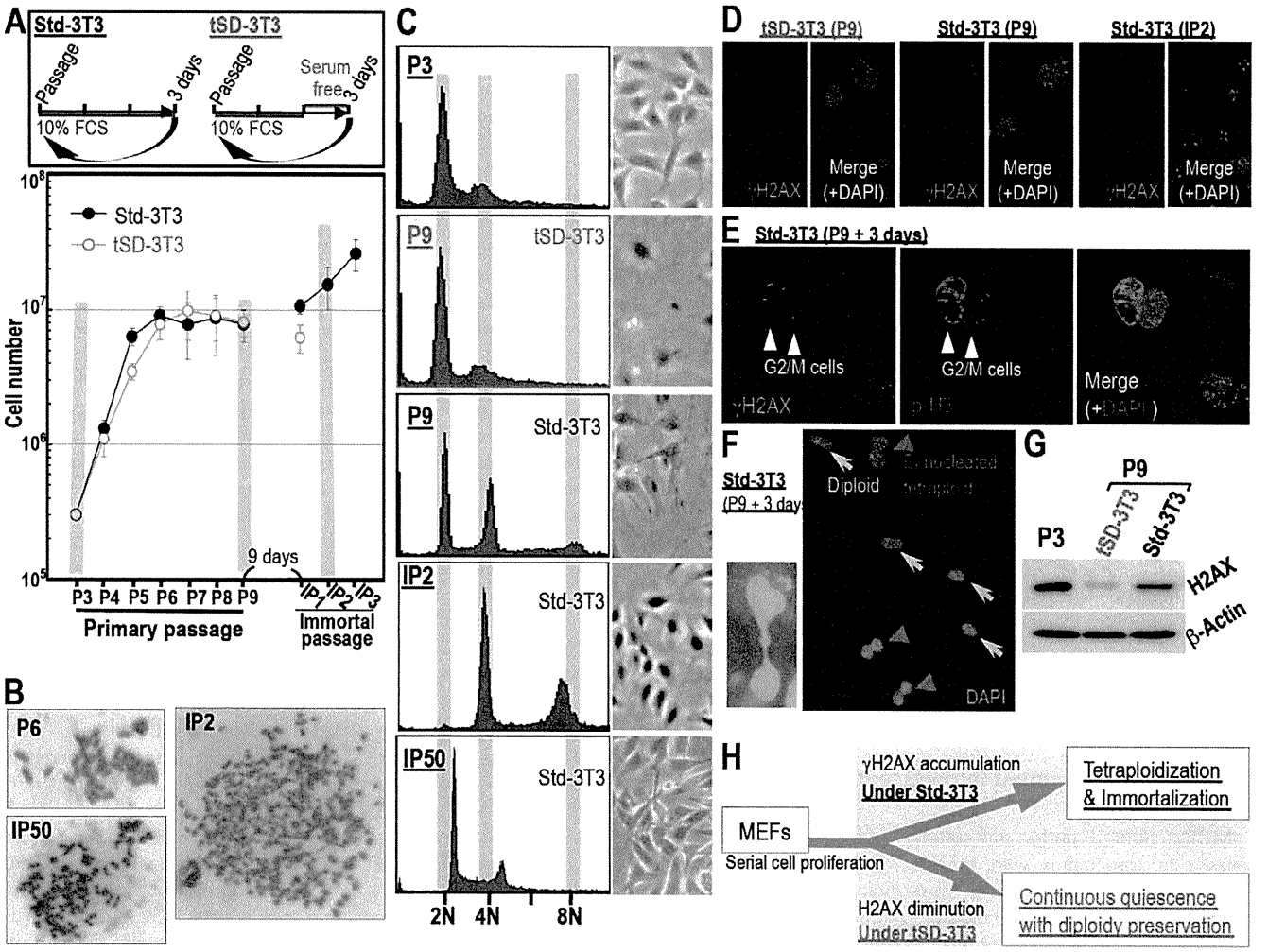

Figure 1. Immortality with tetraploidy is blocked in quiescent cells with diploidy, diminished H2AX, and no γH2AX foci. A. Growth curves of MEFs cultured under the standard 3T3 protocol (Std-3T3) or the T3 protocol with temporary serum deprivation (tSD-3T3) as schematically shown. MEFs under Std-3T3 conditions were immortalized, whereas MEFs cultured under tSD-3T3 conditions were not. **B** Genomic instability developed in immortalized MEFs (IP2) under Std-3T3 conditions. **C.** Genomic status was determined by flow-cytometry at the indicated conditions and passages. Representative images are shown. Tetraploidy development was blocked under tSD-3T3 conditions, while tetraploidy had already developed in growth-arrested MEFs at P9 under Std-3T3 conditions (see increasing 4N and 8N peaks). **D.** DNA lesions identified by γH2AX foci spontaneously accumulated in MEFs developing tetraploidy and immortality (P9) under Std-3T3 conditions as well as in immortal cells (IP2), while MEFs that maintained quiescent status with genomic stability under tSD-3T3 conditions contained no foci. **E.** DNA lesion-carryover into the G2-M phases was determined for lesions that spontaneously accumulated in senescent MEFs under Std-3T3 conditions. DNA lesions in senescing MEFs are also observed in the G2-M phases determined by phosphorylated H3. **F.** Chromosome bridge formation (Left panel) is observed in association with DNA lesion-carryover into the G2-M phases under Std-3T3 conditions with the resulting accumulation of bi-nucleated tetraploidy (Right panel: red arrow heads). Representative images are shown. **G.** The total H2AX level at P9 under each condition was determined. Whereas a significant reduction in H2AX expression was observed in MEFs with genomic stability under tSD-3T3 conditions, MEFs that developed immortality and genomic instability under Std-3T3 conditions did not show a significant decrease in H2AX expression. **H.** A model of the life-cycle of MEFs undergoing quiescence or developing immortality. While quiescent MEFs preserve diploidy and show diminished H2AX levels, MEFs developing immortality exhibited γH2AX foci accumulation.

doi:10.1371/journal.pone.0023432.g001

expression. In these cells, the H2AX level is less than 100-fold compared to that in actively growing cells. To study the effect of growth stimulation in cells with an H2AX-diminished quiescent status, complete medium (DMEM with 10% FBS) was added to quiescent MEFs prepared under tSD-3T3 conditions (Fig. 3A–C). In these cells, cell-cycle progression was initiated with the expression of PCNA and histones H3 and H2AX, which led to γH2AX foci formation (Fig. 3D, E). Abrogating quiescent status with complete medium resulted in the establishment of immortalized MEFs with tetraploidy (Fig. 3A–C). However, it took 30 days to initiate immortal passage in H2AX-diminished quiescent MEFs, while immortality was acquired in only 9 days for P9 MEFs under Std-3T3 conditions, suggesting that the H2AX-diminished quiescent status protected cells from immortalization. Supporting this argument, primary MEFs transfected with an H2AX expression vector also acquired immortality at an accelerated rate (Fig. S5A–C). Such H2AX-overexpression may induce the effect of DNA replication stress because immortality in H2AX-overexpressing MEFs were again developed with tetraploidy (Fig. S5D,E). Unexpectedly, H2AX status was totally recovered in actively growing, immortalized MEFs (Fig. 3F, G), which illustrates the association of H2AX status with growth activity.

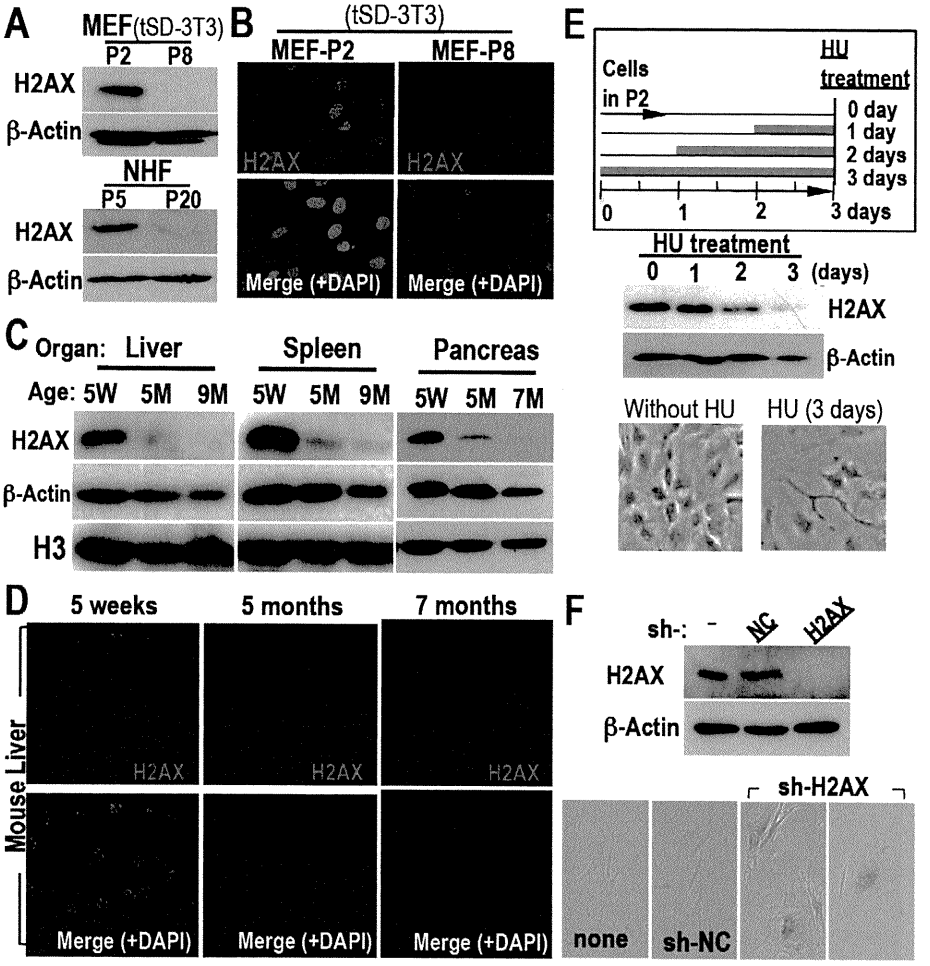

Figure 2. Quiescent cell-status is induced with H2AX diminution both *in vitro* and *in vivo*. **A,B** H2AX expression in growth-arrested cells (P8 for MEFs under tSD-3T3 conditions, P20 for NHFs) was determined by Western blotting (**A**) and immunofluorescent staining (**B**), revealing H2AX diminution in both types of growth-arrested cells. **C,D** H2AX diminution was also measured in adult mice organs by Western blotting (**C**) and in liver sections by immunofluorescent staining (**D**). Samples were prepared from five week (5W), five month (5M) and seven- or nine-month-old mice (7M or 9M). **E.** The involvement of H2AX diminution in DNA damage-induced premature senescence was determined after 0.2 mM HU treatment. Orange bars indicate the periods of HU treatment. Premature damage-induced senescence was observed with H2AX diminution, in which cells were flattened and enlarged, morphology typical of senescent cells. **F.** The effect of H2AX knockdown on senescence was determined in NHFs. Senescence was directly induced by H2AX knockdown in NHFs. H2AX status and senescence was determined by Western blotting (top) and SA-β-gal activation, and cells exhibited a flattened and enlarged morphology (bottoms), respectively.
doi:10.1371/journal.pone.0023432.g002

However, this also poses the question of how the down-regulation of H2AX expression in quiescent MEFs is reversed after immortalization.

Immortalized cells no longer achieve H2AX diminution-associated quiescent status

To explore the effects of the change in H2AX status, the response of H2AX to DNA replication stress was compared between primary and immortalized MEFs. While H2AX in primary MEFs was down-regulated after HU treatment, this did not occur in immortalized MEFs (Fig. 3H), which indicates that H2AX diminution-associated quiescent cell status is not inducible after immortalization. Thus, quiescent status is preserved in cells with diminished H2AX expression and stable diploidy but is abrogated under continuous growth stimulation, inducing cell cycle progression and γH2AX foci formation, and eventually leading to immortality with tetraploidy and H2AX recovery. Since the Arf/p53 module is specifically mutated during MEF immortalization [22], p53 might be involved in H2AX down-regulation. In fact, unlike senescent normal cells, H2AX expression is relatively high (2–20% of total H2A) in cancer cells as well as in growing NHFs (10%) [28].

H2AX diminution-associated quiescent status is produced by p53 and prohibits the development of immortality

To determine the involvement of p53 in H2AX down-regulation, *p53* knockout (KO) MEFs were cultured. Unlike normal primary MEFs, but similar to immortalized MEFs (Fig. 3H), H2AX expression in primary *p53*-KO-MEFs was not decreased by HU treatment (Fig. 4A). Furthermore, *p53*-KO-MEFs continuously grew, without change in H2AX status even under tSD-3T3 conditions (Fig. 4B, C). This indicates that H2AX in wild-type (WT)-MEFs is down-regulated by p53 to

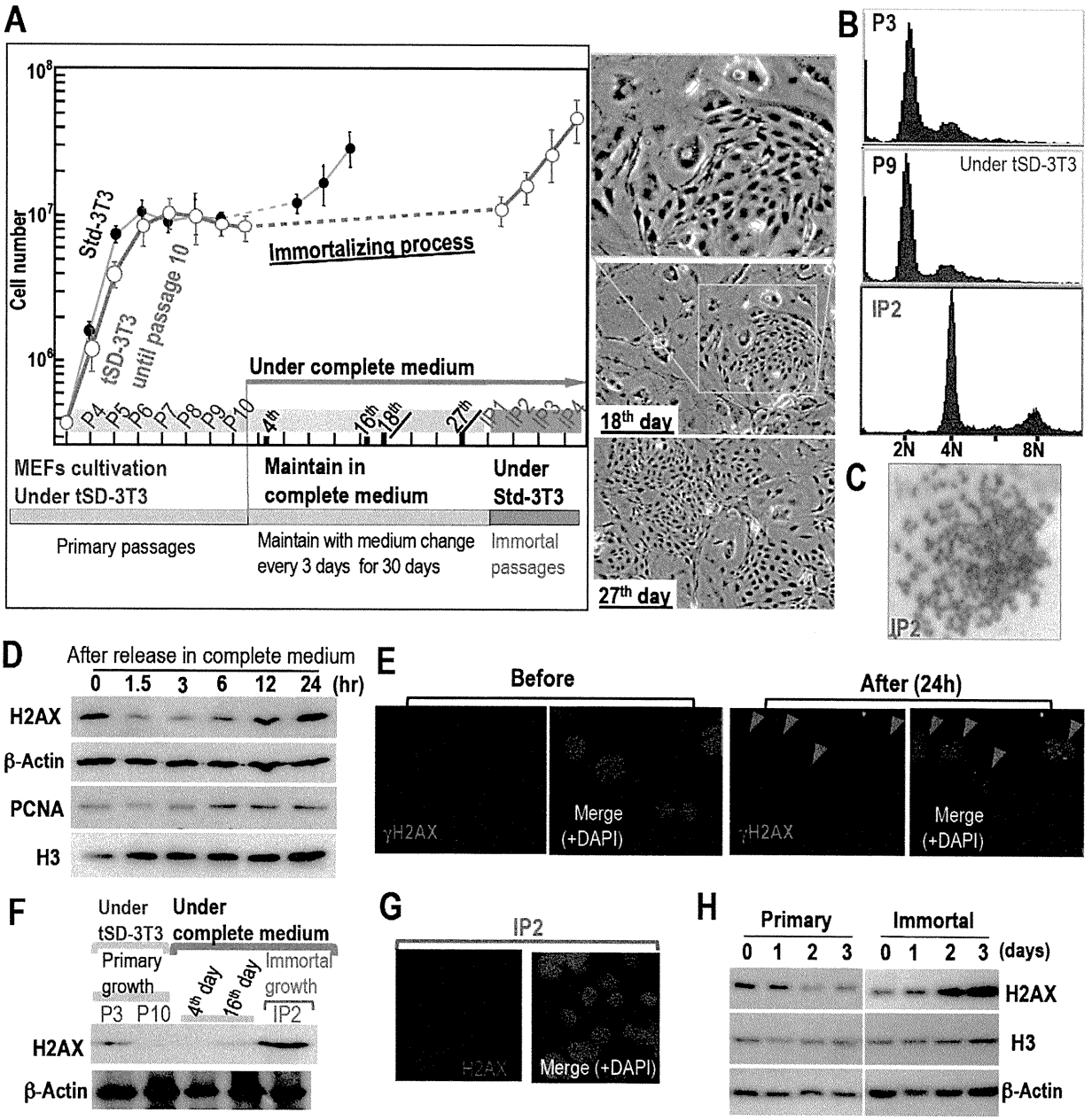

Figure 3. H2AX-diminished quiescent cell-status is abolished by continuous growth stimulation with accompanying H2AX recovery. A. Quiescent MEFs with diminished H2AX expression were cultured under tSD-3T3 conditions until P10. They were then exposed to complete medium, which was changed every three days for 30 days. Immortal passages were started under Std-3T3 conditions (red circles). MEFs cultured under the Std-3T3 conditions (black circles) as in Figure 1a were superimposed for comparison of the time needed to acquire immortality. Representative images of MEFs during the process of acquiring immortality are also shown. **B,C.** Tetraploidy development in immortalized MEFs (IP2) was observed by flow-cytometry (**B**) and Giemsa staining (**C**). **D.** Growth acceleration-associated cell cycle progression and H2AX induction. To determine the effect of serum induction on H2AX expression and cell cycle progression, senescent MEFs at P8 were incubated in serum-free medium for 24 h and harvested after exposure to complete medium for various times. H2AX expression increased with increasing PCNA and histone H3, which suggests that the expression of these chromatin factors was associated with S phase entry. To detect H2AX levels in these MEFs at P8, the H2AX signal was visualized by longer exposure. **E.** DNA lesions characterized by γH2AX foci were induced in MEFs (red arrowheads) after exposure to complete medium as in **D**. **F,G.** H2AX status in immortalized MEFs was determined by Western blotting (**F**) and immunofluorescence (**G**), revealing H2AX recovery. **H.** DNA replication stress-associated H2AX diminution was compared between normal and immortalized MEFs as in Figure 2E, in which H2AX was not down-regulated after immortalization.
doi:10.1371/journal.pone.0023432.g003

induce cellular quiescence and is recovered in immortalized MEFs in association with tetraploidization and mutation of the Arf/p53 module. Although *p53*-KO-MEFs did not undergo H2AX diminution-mediated growth arrest, these MEFs still exhibited a senescent morphology (Fig. 4D, see P8) and subsequently achieved an immortalized morphology (P14), which suggests the immortalization of *p53*-KO-MEFs via the senescent stage without growth arrest. This also indicates that a quiescent cell status is induced by p53 to protect cells from immortality.

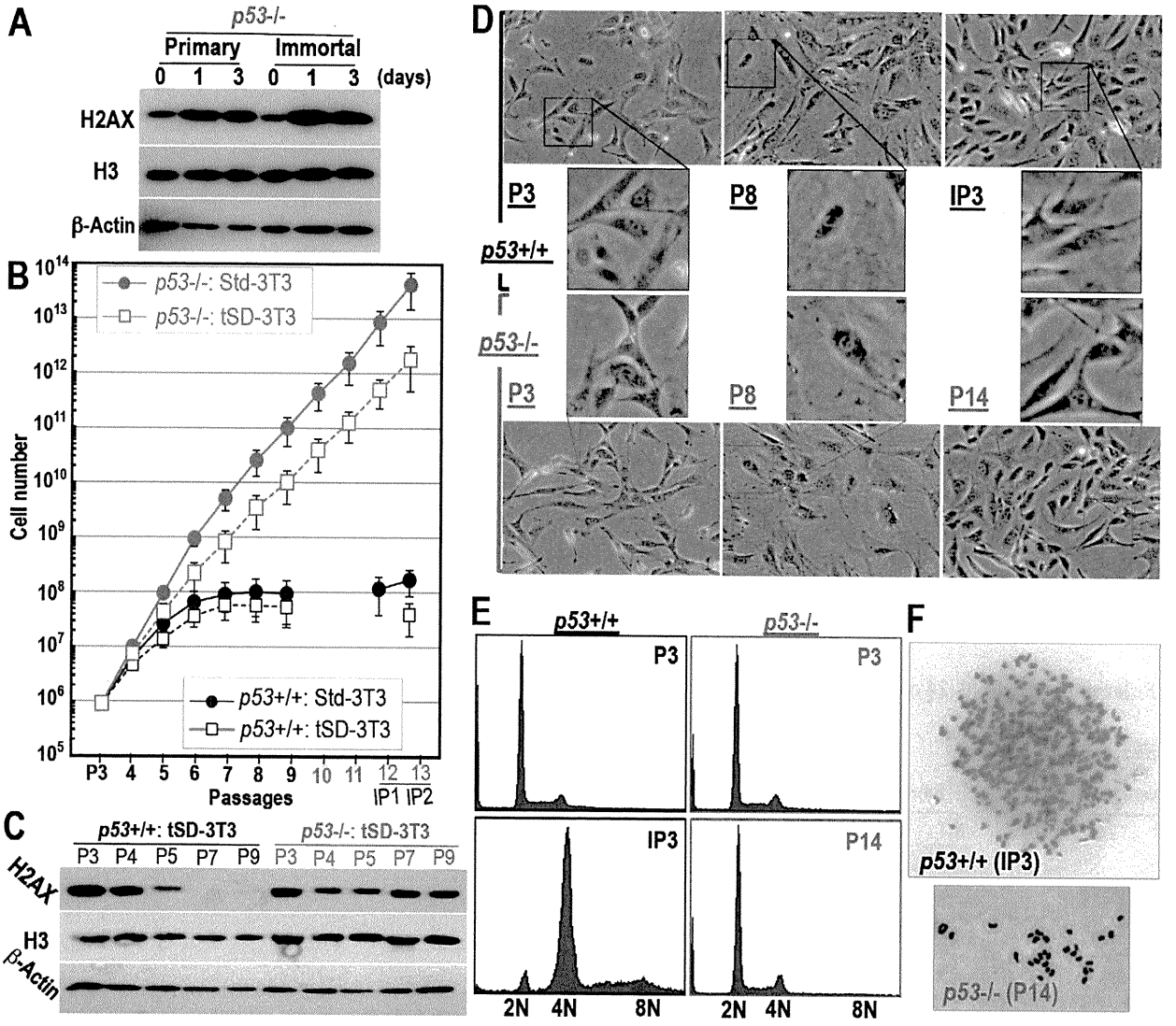

Figure 4. H2AX-diminished quiescent cell status is regulated by p53. A. DNA replication stress-associated H2AX diminution status was determined in *p53*-KO MEFs as in Figure 2E, in which H2AX was not down-regulated, even in primary MEFs. **B–F.** Primary *p53*-KO MEFs were cultured during the senescing and immortalizing processes (**B**). H2AX status was determined by Western blotting (**C**), morphological assessment (**D**), genomic status determined by flow-cytometry (**E**), and chromosome spread (**F**). Although *p53*-KO MEFs never showed major changes in H2AX expression, tetraploidization or growth arrest, *p53*-KO MEFs still exhibited a senescent morphology (P8) before achieving an immortalized morphology (P14).
doi:10.1371/journal.pone.0023432.g004

Mutation of the Arf/p53 module is induced with tetraploidization, triggered by DNA replication stress under moderately decreased H2AX levels in normal cells

Whereas *p53*-KO-MEFs are immortalized with diploidy (Fig. 4E, F), WT-MEFs are never immortalized only after tetraploidization [10] (Fig. 1B, C; Fig. 3B, C; Fig. 4E, F) and loss of Arf/p53 [22]. This suggests that the mutation of the Arf/p53 module in WT-MEFs is induced during tetraploidization. Supporting this argument, p53-dependent quiescence produced by diminished H2AX is maintained under diploidy preservation but abrogated after tetraploidization with mutation in the Arf/p53 module and the resulting H2AX recovery (Fig. 3). Therefore, normal WT-MEFs are protected from immortalization by a quiescent cell status, as long as the genome is preserved in diploidy. However, under continuous growth stimulation, tetraploidization also spontaneously arises in WT-MEFs but, unexpectedly, not in *p53*-KO-MEFs.

As tetraploidization was observed at the senescent stage under conditions of continuous growth stimulation that induce DNA replication stress (Fig. 3), the underlying reason for tetraploidization in WT-MEFs but not in *p53*-KO-MEFs might be associated with the repair deficiency that also occurs in an H2AX-diminished background. To examine the tetraploidization risk under an H2AX-diminished background, MEFs of each type were treated with HU for 36 hours and the incidence of bi-nucleated tetraploidy formation was compared (Fig. 5A). As expected, HU treatment-associated H2AX diminution (Fig. 2E) resulted in tetraploidization in primary WT-MEFs but not in immortalized WT-MEFs or p53-KO-MEFs (Fig. 5A). Thus, although normal cells become quiescent with largely diminished H2AX under diploidy, senescing cells with residual H2AX under growth stimulating conditions are potentially at risk of developing tetraploidy in response to DNA replication stress.

Finally, to address changes in DNA replication stress-sensitivity during serial proliferation of normal MEFs, the repair efficiencies

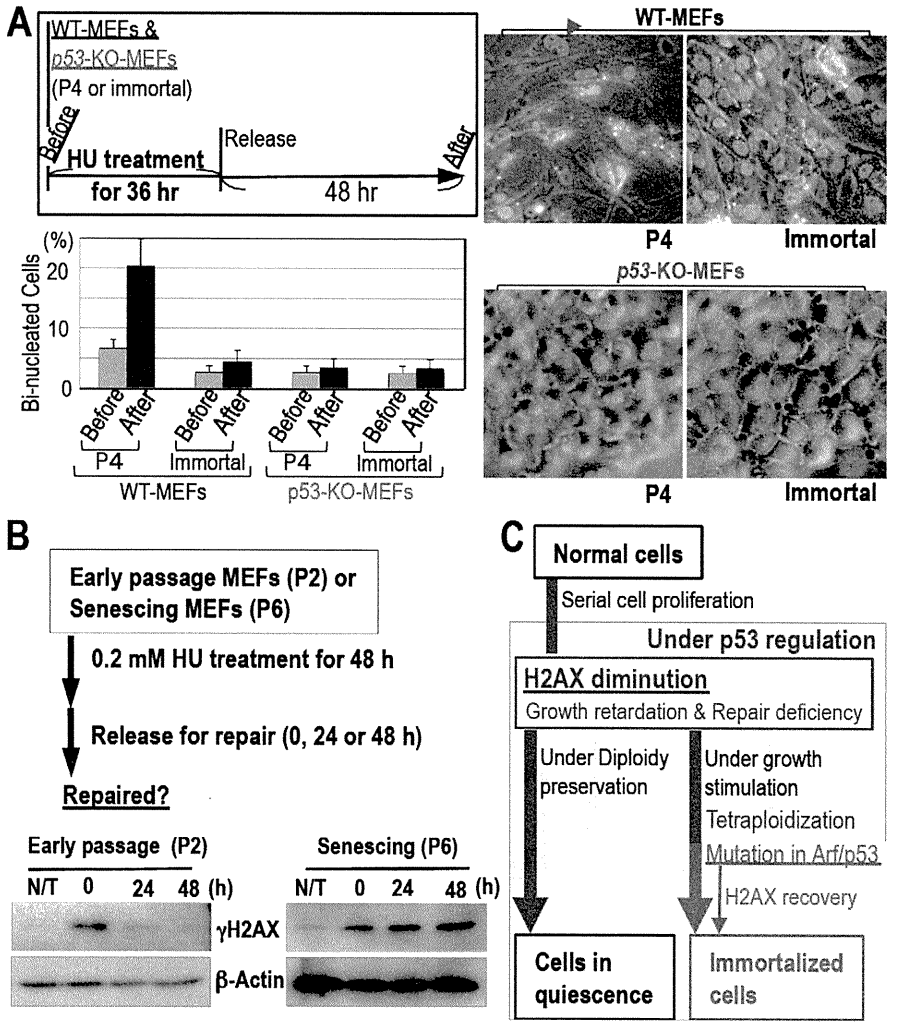

Figure 5. Increased risk of tetraploidization in normal MEFs. A. DNA replication stress-associated tetraploidization was determined in MEFs (P4) with the formation of bi-nucleated tetraploidy (red arrowhead) after 0.2 mM HU treatment as illustrated (top-left panel). Tetraploidization was efficiently induced during primary growth but not in immortalized MEFs or *p53*-KO-MEFs. **B.** Repair efficiencies of DNA replication stress-associated lesions were compared between early passage (P2) and senescing MEFs (P6) after 48 h hydroxyurea (HU) treatment. γH2AX signal was used as a marker of DNA lesions, in which γH2AX signal and β-Actin signals in senescing MEFs (P6) were detected only with over-exposure compared to early passage MEFs (P2), due to decreased H2AX levels during senescence. The reduction in γH2AX signal after release was only evident in early passage MEFs, which suggests that senescing cells are defective in resolving DNA replication stress. **C.** A model of MEFs under serial cell proliferation either undergoing quiescence or developing immortality. While MEFs that maintain quiescence and diploidy show diminished H2AX levels, MEFs developing immortality accumulate γH2AX foci.
doi:10.1371/journal.pone.0023432.g005

of DNA replication stress-associated lesions were compared between early passage and senescent MEFs with the decay of the γH2AX signal after release from HU treatment (Fig. 5B). Unlike early passage MEFs (P2), senescing MEFs (P6) were deficient in repairing HU-associated DNA lesions (Fig. 5B), in which MEFs show slow cell-cycle progression and residual H2AX expression. This is in contrast to quiescent MEFs with largely diminished H2AX level that show neither detectable cell cycle progression nor DNA replication stress. Thus, normal cells under serial proliferation decrease H2AX expression; thereby, cells slow growth activity and become defective in DNA repair. In such cells, cellular homeostasis is preserved by quiescence under largely diminished H2AX level regulated by p53 as long as diploidy is preserved. However, these cells are simultaneously at increased risk of tetraploidization with p53 dysfunction under continuous growth acceleration, resulting in the development of immortality and recovery of H2AX activity and cell growth (Fig. 5C).

Discussion

The results of this study revealed the following novel concepts: (i) normal cells generally achieve quiescent status with diminished H2AX level both *in vitro* and *in vivo*, and this is regulated by p53; (ii) growth arrested normal cells with senescent morphology can be defined as either (a) those in a continuous quiescent status with largely diminished H2AX level or (b) those in a transient status with inducing genomic instability and the resulting onset of immortality, under which cells accumulate γH2AX foci; (iii) to protect cells from immortality, one of the critical roles of p53 is the induction of growth-arrest via the down-regulation of H2AX with cellular quiescence. Cells in H2AX diminution-associated quiescence are shown in the cause of mature and premature senescence, during which cells show senescent morphology (Fig. S1), probably because these cells are repair defective (Fig. 5B). However such repair deficiency is also associated with genomic instability

development under accelerated growth stimulation, resulting in immortality acquisition with Arf/p53 module mutation and H2AX recovery.

Since growth-arrested cellular status with senescent morphology is directly induced by H2AX-knockdown (Fig. 2F), H2AX down-regulation is involved in a cause of quiescent cellular status. On the other hand, residual H2AX-expression in senescent cells is an associated effect for tetraploidization and immortalization: residual H2AX in senescent cells are only observed under accelerated growth stimulation (Figs. 1 and 3), under which cells are subjected to DNA replication stress and exhibit γH2AX, resulting in tetraploidization. Thus, even though cells are morphologically senescent with no growth in total cell number, cellular statuses could be either cells developing genomic instability under continuous growth acceleration (Std-3T3) or continuously quiescent cells under occasional arrest (tSD-3T3).

Unlike highly accumulated p53 that induces apoptosis, the Arf/p53 module under normal conditions functions for longevity by suppressing tumors in mice and giving protection from immortalization in MEFs [22]. Here, our results illustrated that such cellular status is produced with H2AX diminution-associated quiescence by protecting from immortalization under normal p53 regulation but is abrogated by Arf/p53 module mutation that is induced with tetraploidization under continuous growth stimulation, resulting in recovery of H2AX and growth activity. Unlike cells undergoing apoptosis, cells preserving quiescence under normal conditions do not accumulate p53 protein [10], which is probably associated with p53 function expression for quiescent status preservation but not for apoptosis induction. Intriguingly, such p53-dependent H2AX diminution was only observed after cells reach growth arrest both *in vivo* and *in vitro* but not growing cells in early passages and in organs from young mice (Fig. 2). In accordance with this, the expression of p53 targets Sidt2 and Phlda3, which are likely associated with tumor suppression [32], were elevated after cells become H2AX diminution-associated quiescent (P7) compared to cells in early passage (P3) (Fig. S6). However, similar to p53 protein, the increase in p53 transcript is also limited (Fig. S6). Thus, p53 function is expressed for apoptosis with accumulated p53, otherwise for H2AX-diminution associated quiescent status preservation under normal regulation without accumulating p53.

Except for tumors associated with specific chromosomal translocation, development of most cancers as well as *in vitro* cellular transformation is associated with genomic instability of either CIN or MIN [2,3]. Importantly, tetraploidization, a major initial form of CIN under a mismatch repair proficient background is induced with oncogenic stress by accelerated S-phase entry [10], leading to immortality acquisition in MEFs with mutation in the Arf/p53 module. Here, our results showed that quiescence could be preserved with largely diminished H2AX and diploidy preservation under the regulation of p53. Although H2AX down-regulation is only observed under functional p53 regulation, it is still unclear how p53 down-regulates H2AX. Our results showed the reduction of total H2AX transcript during the senescing process (Fig. S4) and a damage-induced decrease of H2AX protein under functional p53 regulation (Fig. 2E; Fig. 4A, B). Although p53 role for H2AX down-regulation is unclear, the regulation might be indirect because (1) there is no p53-binding site on the *H2AX* promoter, (2) there is no signal of the *H2AX* gene with ChIP-on-CHIP analyses against p53 [33], (3) H2AX expression does not associate with the activation level of p53 as we observed no association between H2AX expression and p53 activation (Fig. S7).

Together, our results provide a rationale for the regulation of cellular homeostasis preservation. By prohibiting immortality development and preserving quiescent cell status, p53 induces an H2AX diminution-mediated quiescent status. However, this status is abrogated by continuous growth stimulation, which results in the induction of genomic instability with mutation of the Arf/p53 module, which leads into H2AX recovery, the restoration of growth activity, and immortality acquisition (Fig. 5C).

Methods

Ethics Statement

Mice were treated in accordance with the Japanese Laws and the Guidelines for Animal Experimentation of National Cancer Center. All experiments were approved by The Committee for Ethics in Animal Experimentation of National Cancer Center (approval ID numbers: A59-09 and T07-038).

Cell culture and tissue samples

Cells were cultured as described previously [34]. Both wild-type and *p53*-KO MEFs were prepared from day 13.5 embryos of wild type and $p53^{(+/-)}$ mice [35] as previously described [34] and cultured under the standard 3T3 (Std-3T3) passage protocol [36] or with the following modifications: tSD-3T3. Senescing MEFs (P6 or P8) were maintained under tSD-3T3 conditions for the experiments shown in Figures 2, 3, 4, 5. NHFs (normal human umbilical cord fibroblasts; HUC-F2, RIKEN BRL Cell Bank) were cultured under Std-3T3 conditions. Resveratrol treatment of NHFs was performed as for MEFs. For the H2AX shRNA study, the reported sequence oligonucleotide [37,38] was inserted into the pSuper.retro.puro vector (Oligoengine) and the shRNA virus was then prepared using 293T cells. The virus was infected into NHF cells and selected with puromycin. Mouse tissue samples were prepared from mice at the ages indicated (Sankyo Labo Service).

DNA damage and induction of replication stress

DSB damage was induced by neocarzinostatin (Pola Pharma, Tokyo, Japan) treatment. For induction of DNA replication stress, MEFs were treated with hydroxyurea (HU).

Antibodies, immunostaining and Western blotting

Antibodies against γH2AX (JBW301, Upstate Biotechnology) and H2AX (Bethyl) were used for immunostaining and Western blot analysis. Antibodies against β-actin (AC-74, Sigma), PCNA (Santa Cruz) and histone H3 (ab1791, Abcam) were used for Western blot analysis. Prior to immunostaining with primary and secondary antibodies, cells were fixed with 4% paraformaldehyde for 10 min and permeabilized with 0.1% Triton X-100/PBS for 10 min. Western blot analysis and confocal microscopy were performed as described previously [10].

Transcription level analyses with RT-PCR

Total RNA was extracted from MEFs with the RNeasy system (Sigma). RNA (0.8 μg) was reverse-transcribed using a cDNA Archive kit (Applied Biosystems) and subjected to PCR. The following PCR primers were used: H2axf, 5′-TTGCTTC-AGCTTGGTGCTTAG-3′; H2axr, AACTGGTATGAGGC-CAGCAAC; β-actinf, CATCCAGGCTGTGCTGTCCCTGTA-TGC; and β-actinr, GATCTTCATGGTGCTAGGAGCCA-GAGC; Trp53-F, CGGATAGTATTTCACCCTCAAGATC-CG; Trp53-R, AGCCCTGCTGTCTCCAGACTC; Sidt2-F, CGGAAGGCTGGTTTCTGAGTTTCCG; Sidt2-R, CTGTA-AACGCCAAGGACCAGAA; Phlda3-F, CGGTCCATCTAC-

TTCACGCTAGTGACCG; Phlda3-R, TGGATGGCCTGTTGATTCTTGA; Gapdh-F, AACTTTGGCATTGTGGAAGG; Gapdh-R, ATGCAGGGATGATGTTCTGG. The amplified products by Ampli*Taq* Gold (Applied Biosystems) were separated on a 2% agarose gel and visualized with ethidium bromide. Otherwise, real-time PCR assay was carried out using Power SYBER green PCR Master kit (ABI).

Chromosome spreads

Mitotic cells were prepared by treatment with 20 ng/ml nocodazole for 6 h and then collected. The collected cells were swollen hypotonically with 75 mM KCl for 15 min, and then fixed with Carnoy's solution (75% methanol/25% acetic acid) for 20 min. After changing the fixative once, the cells were dropped in Carnoy's solution onto glass slides and air-dried. The slides were stained with 4% Giemsa (Merck) solution for 10 min, washed briefly in tap water, and air-dried.

Supporting Information

Figure S1 Representative images of MEFs during the lifespan. MEFs cultivated as in Figure 1A top lead into either immortality development under Std-3T3 or quiescence preservation under tSD-3T3. After serial cultivation, MEFs become morphologically senescent, i.e., flattened and enlarged morphology (P9) under both Std-3T3 and tSD-3T3 conditions. While continuous MEF-culture under tSD-3T3 preserved the quiescent status with continuously senescent morphology, continuous MEF-culture under Std-3T3 lead to the sporadic emergence of immortalized colony from the senescent MEFs. Immortalized MEFs (IP2) are morphologically escaped from senescence and rather similar to that in early passage (P3).
(TIF)

Figure S2 H2AX diminution is also observed in adult mice organs. Samples were prepared from five week (5W), five month (5M) and seven- or nine-month-old mice (7M or 9M). Compared to five months old organs, H2AX protein level is diminished in Testis (9M), Brain (7M), and Colon (7M), in which the diminution levels are lower than those in Liver, Spleen, and Pancreas. In Heart and Thymus, H2AX levels did not altered the alteration in through 5 weeks old to 7 or 9 months old.
(TIF)

Figure S3 H2AX diminution is also shown in damage induced premature senescence. Premature senescence was induced with NCS treatment as shown schematically in the top, in which each red arrowhead represents 100 ng/μl NCS treatment. Premature senescence by damage was induced with H2AX diminution, in which cells showed typical senescent morphology of flattened and enlarged.
(TIF)

Figure S4 H2AX transcript is decreased in quiescent MEFs. Decrease in H2AX mRNA level in senescing MEFs was observed by RT-PCR (right panel) and is compared with protein diminution (left panel).
(TIF)

Figure S5 H2AX over-expression accelerates immortality development in MEFs with tetraploidy. A. Experimental scheme of H2AX over expression. After transfection of H2AX-over expressing (H2AX-OE) or empty control vectors into early passage MEFs (P3), the transformed MEFs were selected, re-plated, and maintained in complete medium until immortalized cells appeared. **B.** Growth curves of MEFs during the experiments in A. MEFs before transfection and re-plating, MEFs transfected with H2AX-over-expressing vector, and MEFs transfected with empty control vector are indicated by black closed squares, red open circles, and black open diamonds, respectively. MEFs over-expressing H2AX showed accelerated development of immortality. **C.** H2AX status was determined as indicated in the figure. Although senescence was induced in the transfected and selected MEFs, H2AX over-expressing MEFs show higher levels of H2AX after the selection resulting in the development of immortality with H2AX recovery. **D.** Representative MEF images during accelerated immortality development with H2AX over-expression and controls. MEFs transfected with the H2AX over-expressing vector showed an efficient escape from senescence, while MEFs carrying the negative control vectors remained senescent with a flattened and enlarged morphology. **E,F.** Genomic instability status in immortalized MEFs (IP3) that were developed with H2AX over-expression was assessed by flow-cytometry (**E**) and Giemsa staining of M-phase chromosome (**F**).
(TIF)

Figure S6 p53 expression in senescing MEFs. To determine p53 expression in the cause of senescence, the expression levels of p53 and the targets (Sidt2 and Phlda3) that are likely associated with tumor suppression were compared between early passage (P2) and senescent MEFs (P7) under tSD-3T3 conditions. Along with H2AX diminution under p53 proficient background after serial cultivation, the expressions of Sidt2 and Phlda3 were observed in senescent MEFs (P7), in which the change in the expressed p53 transcript is limited.
(TIF)

Figure S7 p53 activation shown by miR34a expression in primary wt-MEFs after damage is not directly associated with H2AX expression levels at least for transcript regulation. A. To confirm p53 dependent DNA damage response, wt- and $p53^{-/-}$-MEFs in primary and immortal were treated with 200 ng/ml neocarzinostatin (NCS) for 6 hours and the expression of p53-target miR34a was assessed. As expected, miR34a expression was shown after NCS treatment in primary wt-MEFs (wild type) but neither in immortalized wt-MEFs nor in $p53^{-/-}$-MEFs. **B.** To determine the p53-activation associated change in the expression levels of H2AX transcript, mRNA levels of H2AX in MEFs treated as in **A** were analyzed. Whereas p53 is activated after NCS treatment in primary wt-MEFs, H2AX transcript levels were stable, suggesting no direct regulation by p53 transcription factor for H2AX expression. The PCR primers for miR34a were used from miRNA-specific primers (ABI) with snoRNA202 (ABI) for the control. Real-time PCR assay was carried out TaqMan microRNA assay kit (ABI).
(TIF)

Acknowledgments

We thank RIKEN BRL Cell Bank for the normal human umbilical cord fibroblast (NHF) cells (HUC-F2). We also thank K. Shimizu-Saito, M. Yanokura, and I. Kobayashi for technical support. We are grateful to S. Takeda, W. Bonner, P. Hsieh, K. Okamoto, and S. Nakada for critical reading of the manuscript and to T. Tsuzuki and Y. Nakatsu for critical discussion of the study.

Author Contributions

Conceived and designed the experiments: KY. Performed the experiments: YA H. Fuji H. Fukuda AI KS YY MS YI JU KY. Analyzed the data: H. Fuji KY. Contributed reagents/materials/analysis tools: SM NT YH HN MM. Wrote the paper: KY H. Fukuda HT.

References

1. Negrini S, Gorgoulis VG, Halazonetis TD (2010) Genomic instability–an evolving hallmark of cancer. Nat Rev Mol Cell Biol 11: 220–228.
2. Lengauer C, Kinzler KW, Vogelstein B (1997) Genetic instabilities in colorectal cancers. Nature 386: 632–627.
3. Lengauer C, Kinzler KW, Vogelstein B (1998) Genetic instabilities in human cancers. Nature 396: 643–649.
4. Stephans PJ, Greenman CD, Fu B, Yang F, Bignell GR, et al. (2011) Massive genomic rearrangement acquired in a single catastrophic event during cancer development. Cell 144: 27–40.
5. Vitale I, Galluzzi L, Senovilla L, Criollo A, Jemaà M, et al. Illicit survival of cancer cells during polyploidization and depolyploidization. Cell death differ, doi: 10.1038/cdd.2010.145.
6. Danes BS (1978) Increased in vitro tetraploidy: tissue specific within the heritable colorectal cancer syndromes with polyposis coli. Cancer 41: 2330–2334.
7. Dutrillaux B, Gerbault-Seureau M, Remvikos Y, Zafrani B, Prieur M (1991) Breast cancer genetic evolution: I. Data from cytogenetics and DNA content. Breast Cancer Res Treat 19: 245–255.
8. Heselmeyer K, Schröck E, du Manoir S, Blegen H, Shah K, et al. (1996) Gain of chromosome 3q defines the transition from severe dysplasia to invasive carcinoma of the uterine cervix. Proc Natl Acad Sci USA 93: 479–484.
9. Maley CC, Galipeau PC, Li X, Sanchez CA, Paulson TG, et al. (2004) The combination of genetic instability and clonal expansion predicts progression to esophageal adenocarcinoma. Cancer Res 64: 7629–7633.
10. Ichijima Y, Yoshioka K, Yoshioka Y, Shinohe K, Fujimori H, et al. (2010) DNA lesions induced by replication stress trigger mitotic aberration and tetraploidy development. PLoS One 5: e8821.
11. Bartkova J, Horejsí Z, Koed K, Krämer A, Tort F, et al. (2005) DNA damage response as a candidate anti-cancer barrier in early human tumorigenesis. Nature 434: 864–870.
12. Gorgoulis VG, Vassiliou LV, Karakaidos P, Zacharatos P, Kotsinas A, et al. (2005) Activation of the DNA damage checkpoint and genomic instability in human precancerous lesions. Nature 434: 907–913.
13. Sedelnikova OA, Horikawa I, Zimonjic DB, Popescu NC, Bonner WM, et al. (2004) Senescing human cells and ageing mice accumulate DNA lesions with unrepairable double-strand breaks. Nature Cell Biol 6: 168–170.
14. Nakamura AJ, Chiang YJ, Hathcock KS, Horikawa I, Sedelnikova OA, et al. (2008) Both telomeric and non-telomeric DNA damage are determinants of mammalian cellular senescence. Epigenetics Chromatin 1: 6.
15. Geigl JB, Langer S, Barwisch S, Pfleghaar K, Lederer G, et al. (2004) Analysis of gene expression patterns and chromosomal changes associated with aging. Cancer Res 64: 8550–8557.
16. Sherr CJ, Weber JD (2000) The ARF/p53 pathway. Curr Opin Genet Dev 10: 94–99.
17. Sherr CJ (1998) Tumor surveillance via the ARF-p53 pathway. Genes Dev 12: 2984–2991.
18. Matheu A, Maraver A, Serrano M (2008) The Arf/p53 pathway in cancer and aging. Cancer Res 68: 6031–6034.
19. Tyner SD, Venkatachalam S, Choi J, Jones S, Ghebranious N, et al. (2002) p53 mutant mice that display early ageing-associated phenotypes. Nature 415: 45–53.
20. Maier B, Gluba W, Bernier B, Turner T, Mohammad K, et al. (2004) Modulation of mammalian life span by the short isoform of p53. Genes Dev 18: 306–319.
21. Varela I, Cadiñanos J, Pendás AM, Gutiérrez-Fernández A, Folgueras AR, et al. (2005) Accelerated ageing in mic deficient in Zmpste24 protease is linked to p53 signalling activation. Nature 437: 564–568.
22. Matheu A, Maraver A, Klatt P, Flores I, Garcia-Cao I, et al. (2007) Delayed ageing through damage protection by the Arf/p53 pathway. Nature 448: 375–379.
23. Parrincello S, Samper E, Krtolica A, Goldstein J, Melov S, et al. (2003) Oxygen sensitivity severely limits the replicative lifespan of murine fibroblasts. Nature Cell Biol 5: 741–746.
24. Bassing CH, Chua KF, Sekiguchi J, Suh H, Whitlow SR, et al. (2002) Increased ionizing radiation sensitivity and genomic instability in the absence of histone H2AX. Proc Natl Acad Sci USA 99: 8173–8178.
25. Celeste A, Petersen S, Romanienko PJ, Fernandez-Capetillo O, Chen HT, et al. (2002) Genomic instability in mice lacking histone H2AX. Science 296: 922–927.
26. Bronson R, Lee C, Alt WF (2003) Histone H2AX: A dosage-dependent suppressor of oncogenic translocations and tumors. Cell 114: 359–370.
27. Bassing CH, Alt FW (2004) H2AX May Function as an Anchor to Hold Broken Chromosomal DNA Ends in Close Proximity. Cell Cycle 3: 149–153.
28. Bonner WM, Redon CE, Dickey JS, Nakamura AJ, Sedelnikova OA, et al. (2008) GammaH2AX and cancer. Nature Rev Cancer 8: 957–967.
29. Tsukuda T, Fleming AB, Nickoloff JA, Osley MA (2005) Chromatin remodelling at a DNA double-strand break site in Saccharomyces cerevisiae. Nature 438: 379–383.
30. Keogh MC, Mennella TA, Sawa C, Berthelet S, Krogan NJ, et al. (2006) The Saccharomyces cerevisiae histone H2A variant Htz1 is acetylated by NuA4. Genes Dev 20: 660–665.
31. Ikura T, Tashiro S, Kakino A, Shima H, Jacob N, et al. (2007) DNA damage-dependent acetylation and ubiquitination of H2AX enhances chromatin dynamics. Mol Cell Biol 27: 7028–7040.
32. Brady CA, Jiang D, Mello SS, Johnson TM, Jarvis LA, et al. (2011) Distinct p53 transcriptional programs dictate acute DNA-damage responses and tumor suppression. Cell 145: 571–583.
33. Ceribelli M, Alcalay M, Viganò MA, Mantovani R (2006) Repression of new p53 targets revealed by ChIP on chip experiments. Cell Cycle 5: 1102–1110.
34. Yoshioka K, Yoshioka Y, Hsieh P (2006) ATR kinase activation mediated by MutSα and MutLα in response to cytotoxic O6-methylguanine adducts. Mol Cell 22: 501–510.
35. Tatemichi M, Tazawa H, Masuda M, Saleem M, Wada S, et al. (2004) Suppression of thymic lymphomas and increased nonthymic lymphomagenesis in Trp53-deficient mice lacking inducible nitric oxide synthase gene. Int J Cancer 111: 819–828.
36. Todaro GJ, Green H (1963) Quantitative studies of the growth of mouse embryo cells in culture and their development into established lines. J Cell Biol 17: 299–313.
37. Lukas C, Melander F, Stucki M, Falck J, Bekker-Jensen S, et al. (2004) Mdc1 couples DNA double-strand break recognition by Nbs1 with its H2AX-dependent chromatin retention. EMBO J 23: 2674–2683.
38. Dimitrova N, de Lange T (2006) MDC1 accelerates nonhomologous end-joining of dysfunctional telomeres. Genes Dev 20: 3238–3243.